Electronic Supplementary Information

for New Journal of Chemistry

Nb_2O_5 Supported on Mixed Oxides Catalyzed Oxidative and Photochemical Conversion of Anilines to Azoxybenzenes

Gustavo Senra Gonçalves De Carvalho,[a] Luciano Honorato Chagas,[b] Carla Grijó Fonseca,[a] Pedro Pôssa de Castro,[a] Antônio Carlos Sant'Ana,[a] Alexandre Amaral Leitão,[a] and Giovanni Wilson Amarante [a,*]

[a] Chemistry Department, Federal University of Juiz de Fora, Cidade Universitária, São Pedro, Juiz de Fora, CEP 36036-900, Juiz de Fora, Brazil.

[b] DIPAC/LACAT, National Institute of Technology, Avenida Venezuela, n° 82, Saúde, Rio de Janeiro - RJ, 20081-312.

*giovanni.amarante@ufjf.edu.br

- Summary

1. Catalyst characterization

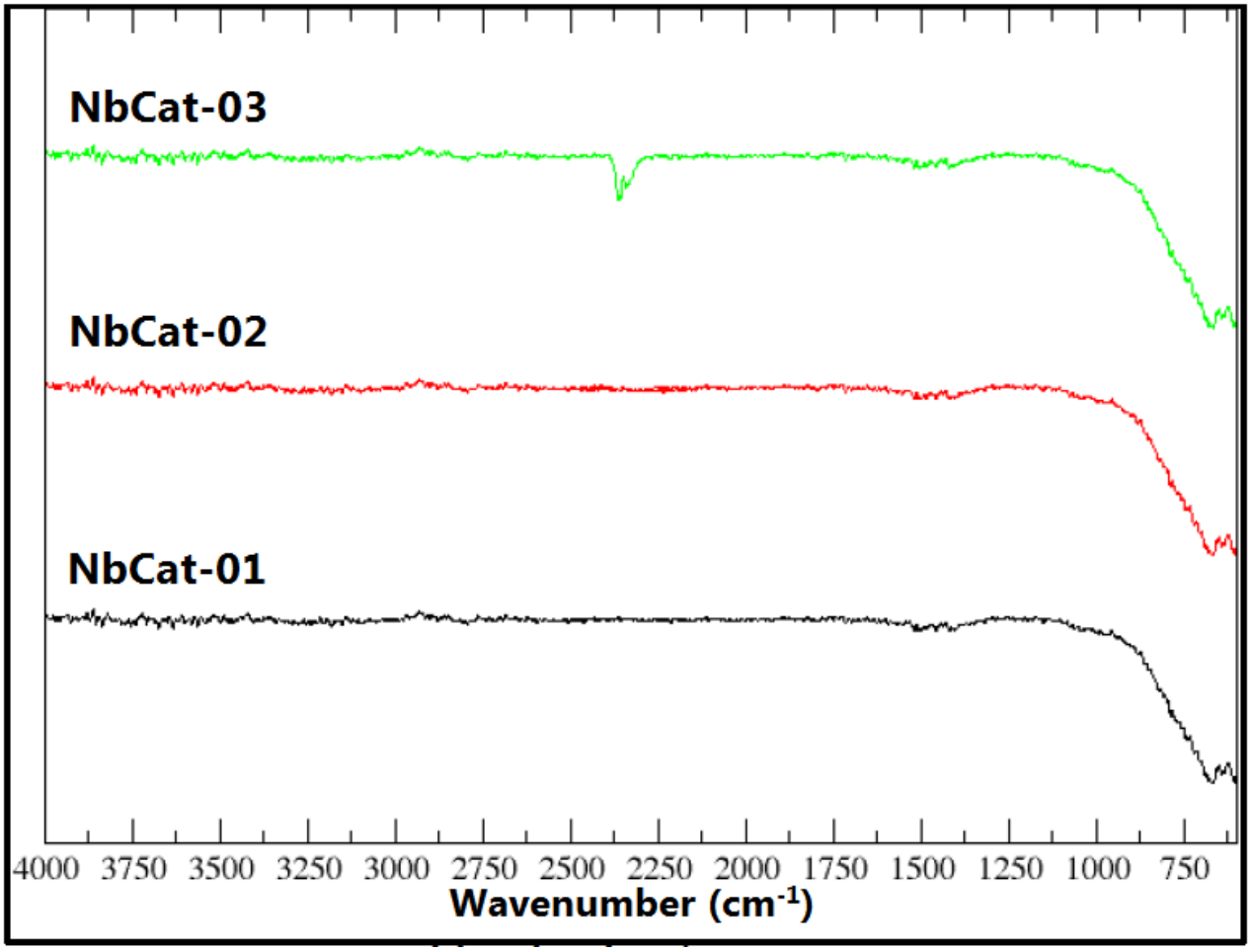

Figure S1. Infrared spectra (KBr) of the niobium supported catalysts.

In order to evaluate the absorption range of the photocatalysts, UV-Vis spectroscopy measurements were performed, noting that the region of greatest absorption in the visible light is violet, blue and green, as shown in the following figure, regions chosen for the tests photocatalytic.

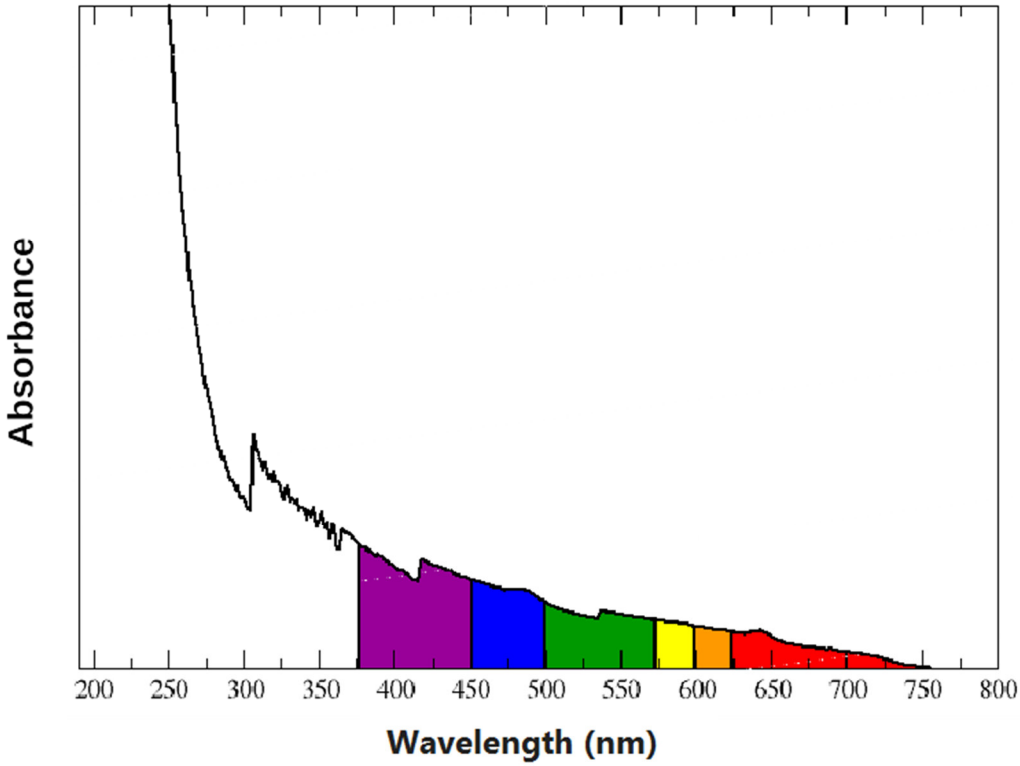

Figure S2. UV-Vis absorbance curve of the **NbCat-02** catalyst.*

* The same absorption profile was also detected for the **NbCat-01** and **NbCat-03** catalysts.

2. Theoretical results for support and catalyst characterization

For the Raman calculations norm-conserving pseudopotentials were adopted [1]. Kohm-Sham orbitals were expanded in a plane waves bases set to a kinetic energy cutoff of 50 Ry and the electron density was obtained at the Γ point in the first Brillouin-Zone of the supercells. The MgO and Spinel structures has cubic symmetry, the parameters, $a = b = c = 4.21$ Å and $\alpha = \beta = \gamma = 90°$, $a = b = c =$ 8.0806 Å $\alpha=\beta=\gamma=90°$ and belong to Fm3m and Fd3m spatial groups respectively [2, 3]. The ZnO has hexagonal symmetry, the following parameters $a = b = 3.2494$ Å, c = 5.2038 Å and belongs to $P6_3mc$ spacial group [4]. In order to construct the slab models, the bulk models were first optimized and the calculated lattice constants showed good agreement with the experimental data. Slab models of the mixed oxides, $ZnAl_2O_4(100)$ and ZnO(001) surfaces were also constructed using periodic boundary conditions and three atomic layers and a vacuum layer of 15 Å in *a* and *c* direction respectively. The vacuum layer was introduced to generate the surface and to ensure that there are no interactions between the periodic images perpendicular to the surface. Considering that it is necessary to maintain the system electroneutrality, on the Al-doped MgO(001) surface two Mg atoms were exchanged by

one Al atom in the first layer and a Mg vacancy was created as done by Alvim *et al.* [5]. The AlZn-doped MgO(001) surface was constructed from the Al-doped MgO(001) surface by the exchange of one Mg atom by one Zn atom. The Al-doped MgO and AlZn-doped MgO surfaces are representative of superficial sites of the Mg/Al mixed oxides. The nomenclature of the surface models used in this work is MgO:Al(001), MgO:AlZn(001), ZnO(001) and $ZnAl_2O_4$(100). The supercells are large enough to avoid interactions among the adsorbed aniline species and its periodic images. Vibrational modes were obtained from calculations of phonons that are based on the harmonic approximation within the Functional Density Perturbation Theory (DFPT) at point q, Γ [6].

Structural characterization by X-ray diffraction of the catalyst supports shown after the LDHs calcination process at 500 °C phases with different degrees of crystallinity. As the DRX patterns corresponding to the mixed oxide phase is very broad, the effective characterization of the compounds that represent the oxides resulting from the calcination is difficult and thus more than one phase may be present. By account, different models of the oxide supports were evaluated, among them, representative models of MgO-type oxides, such as the MgO:Al (001) and MgO:AlZn (001) structures. These structures were generated from magnesium oxide doing isomorphic substitution of Mg by Al and Al and Zn in the surface, a vacancy was generated to neutralize the charge since a cation II is replaced by a III. These models are representative of the local surface sites that must be present in the calcined oxides. Due the difficulties in the structural characterization of the catalyst supports representative models of zincite and spinel ($ZnAl_2O_4$) were also evaluated, since characteristic peaks of these compounds can also be identified.

Besides that, the catalysts used for the photocatalytic reactions has Nb_2O_5, as catalytic phase, which upon being calcined at the temperature of 500 °C become amorphous, so a combined theoretical-experimental study is valuable to identify the most probable structures of the catalyst dispersed on the surfaces. The computational chemistry can provide informations often not accessible by experimental techniques.

In the investigated structures of the NbO and NbOOH clusters the Nb atoms have distorted octahedral coordination when bound to 5 hydroxyl groups and a surface oxygen. Monomers and dimers with variable numbers of Nb=O bonds that are normally associated with Lewis sites and Nb-OH bonds were considered. Possible forms of the clusters (T0, T1, T2, T2-D, T4-D), suggested in different works [7-10], were evaluated and the structures can be visualized in Figure S2. The numbers in the nomenclature of the models refer to the number of Nb = O bonds and the letter D in T2 -D refers to the Nb dimer.

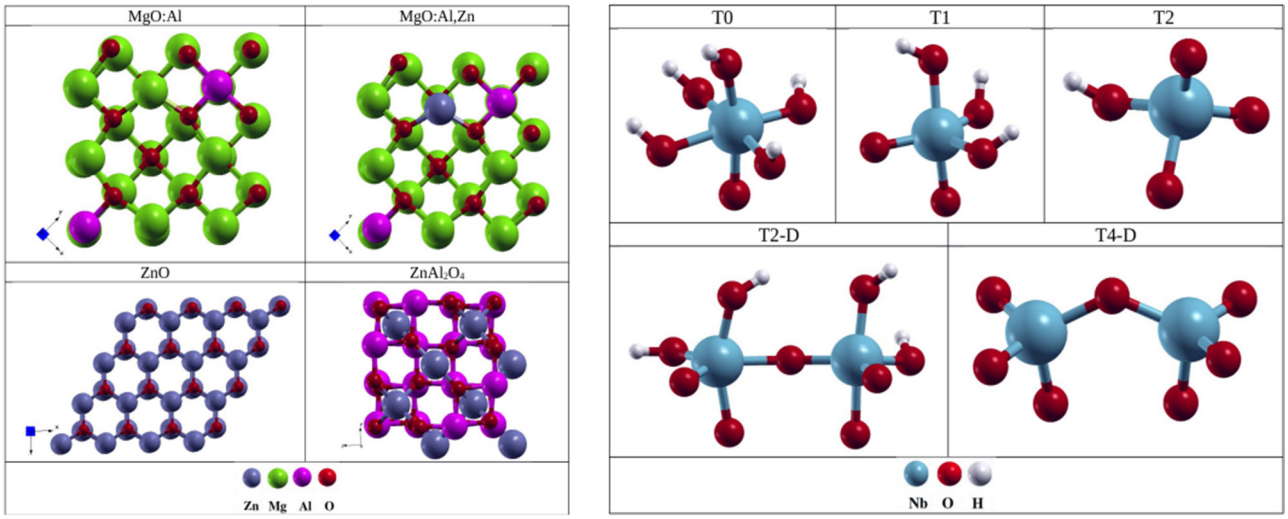

Figure S3. (A) Representative structures of the catalyst support. **(B)** Different geometries optimized for the niobium oxide anchored on the surfaces of oxides from the LDHs calcination.

The main geometric parameters were calculated for the different niobium oxide species in the surface models. The Nb=O bonds have lengths between 1.73 and 1.81 Å. The smaller lengths are observed for the Nb=0 bonds that are not influenced by the surface cations. The length of the Nb-O_{sup} bonds anchoring the monomers and dimmers on the surfaces are in the range of 1.92 to 1.99 Å except for the T0 and T2-D structures anchored on the MgO:AlZn surface, where distances of 2.21 and 2.29 Å were found, respectively, much higher than those observed for the other conformations. The Nb-OH distances range from 1.92 to 2.16 Å, the Nb-OH distances for the isolated hydroxyls that do not interact with the surface cations have the lowest values between 1.92-1.95 Å. The distances observed in the different models are in good agreement with calculations made by Tranca *et al*. [7] for niobium oxide agglomerates on amorphous silica, Nb = O in the range of 1.73 and 1.79 Å and Nb-O bonds in the range of 1.92 to 2.03 Å.

The electronic energies for the anchoring processes described below were used to propose the most stable cluster on each oxide surface. The anchoring process can be described as a reaction between the support and the catalyst precursor with water consumption or release, as done in previous works by Islam *et al*., 2009 and Tranca *et al*., 2015 [7, 9]. The appropriate equations for each model can be seen below:

$$(A)\,Support + H_3NbO_4 + H_2O \rightarrow Support - Nb(OH)_5$$

$$(B)\,Support + H_3NbO_4 \rightarrow Support - ONb(OH)_3$$

$$(C)\,Suport + H_3NbO_4 \rightarrow Support - O_2Nb(OH) + H_2O$$

$$(D)\,Support + 2H_3NbO_4 \rightarrow Support - O_3Nb_2(OH)_4 + H_2O$$

$$(E)\,Support + 2\,H_3NbO_4 \rightarrow Support - O_5Nb_2 + 3\,H_2O$$

From these reactions we can evaluate the formation energy of each of the clusters on the surfaces and compare the stability of each of them. The results were presented in Table S1.

Table S1. Formation energy calculated by means of the respective equations for the anchoring of the different models of Niobium oxides supported on oxide surfaces.

Reactions	**ΔE_{reac} (kcal/mol)**			
	MgO:Al	MgO:Al,Zn	ZnO	$ZnAl_2O_4$
Support + H_3NbO_4 + 1H_2O → Support:T0	-59,82	-71,36	-	-49,85
Support + H_3NbO_4 → Support:T1	-38,28	-43,30	-	-47,12
Support + H_3NbO_4 → Support:T2 + H_2O	-12,14	-30,06	16,37	-
Support + 2H_3NbO_4 → Support:T2-D + H_2O	-74,98	-84,96	-14,60	-78,98
Support + 2H_3NbO_4 → Support:T4-D + 3H_2O	-21,30	-24,76	34,73	-20,52

Obs: The '–' in the table corresponds to models that not converged

According to Table S1, for the four catalyst supports evaluated, the structure Support:T2-D showed the most favored in 0K, these species presented the most negative formation energies. Evaluating the T2-D species on the four supports we noticed that MgO: AlZn is the one that best stabilizes this niobium oxide species (ΔE = -84.96 kcal/mol) followed by $ZnAl_2O_4$ (ΔE = -78,98 kcal/mol), MgO:Al (ΔE = -74.98 kcal/mol) and finally to zincite (-14.60 kcal/mol). These data suggest a high capacity of the supports that contain the cations Al on their surface for the anchoring of the catalysts, possibly being these sites responsible for the stabilization of Nb species and consequently the catalytic activity of these.

For a better understanding of the vibrational analyzes, some simulations were performed using the same structures and the results corroborated with the experimental analyzes previously reported [9] and the results of this work.

Vibrational frequency analysis was also done and the Table S2 shows the calculated vibrations for the considered models and assignment of the normal modes. Only frequencies in the range of 600 to 4000 cm^{-1} were reported.

Table S2. Calculated frequencies for the agglomerates supported on the surface MgO:AlZn, in cm^{-1}.

Models	Frequency	Mode
T0	3595 , 3944	NbO-H stretching
	688, 675	Nb-OH bending
	801	Nb=O
T1	3920, 3969	NbO-H stretching
	618	Nb-OH bending
	933	Nb=O
T2	3958	NbO-H stretching
	722	Nb-O
	668	Nb-OH bending
	816, 869	Nb=O
T2-D	3935, 3615	NbO-H stretching
	671, 646	Nb-OH bending
	947	Nb=O
T4-D	707, 686	Nb-O-Nb
	890	Nb=O

The region between 3000 and 4000 cm^{-1} are dominated by the vibrations of the hydroxyl groups. Values higher than 3600 cm^{-1} are assigned to NbO-H stretching modes (T0, T1 and T2-D models preferably). Raman data for NbOx species supported on Al_2O_3, TiO_2, ZrO_2 and SiO_2 exhibit bands in the region of ~ 825 to ~ 980 cm^{-1} and indicate the existence of Nb=O and Nb-O-Nb bonds [6], the ratio of polymer species to monomeric increasing with niobium loading. EXAFS (Extended X-ray absorption fine structure) studies similarly indicate the presence of species with Nb=O and Nb-O-Nb bonds, as well as Nb-O_{sup} bonds [10]. From the calculations of vibrational frequencies, it was possible to define the vibrational modes related to each frequency. For both monomers and dimers, the frequencies relative to the Nb=O stretch are between 801 and 947 cm^{-1}, however, the highest values are assigned to the free Nb=O bonds, as is the case of MgO:AlZn-T1 and MgO:AlZn-T2-D. Frequencies related to the Nb-O-Nb mode were observed in the range of 686 to 707 cm^{-1}. For high

Nb_2O_5/Al_2O_3 charges a band is observed at ~ 647 cm^{-1} which is characteristic of the mode relative to Nb-O-Nb polymerized bonds [9]. The results obtained for this mode in our calculations are very close to this value. The data obtained from the vibrational analysis are in agreement with data from the literature and with the bands observed in the Raman mapping and used as marker features of the presence of niobium oxide in the catalysts.

In Figure S3, the Raman and IR spectra were presented for the MgO: Al,Zn-T4-D structure, since in this work no bands were observed in the region between 3000 and 4000 cm^{-1}, with the T4-D model being the more likely to be found in the catalytic phase.

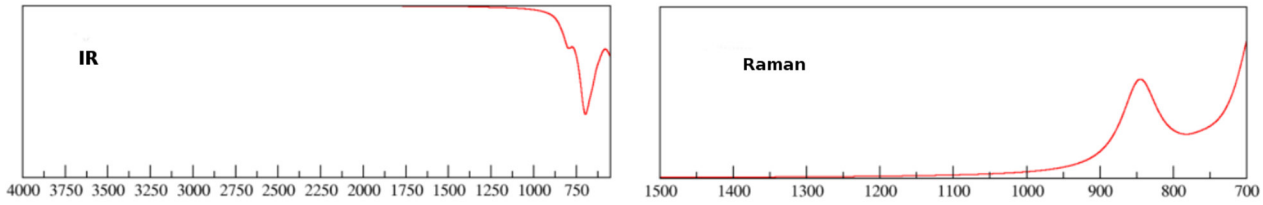

Figure S4. Calculated spectra for the agglomerate (T4-D) supported on the MgO:AlZn surface, in cm^{-1}.

The spectra are in excellent agreement with the experimental Raman spectra. The active vibrational modes in the Raman were observed in the range between 800 and 950 cm^{-1} and bands corresponding to the vibrational modes of the hydroxyl were not observed, only frequencies related to the lattice and Nb-O modes are observed.

Based on a combination of experimental results such as IR, Raman and XRD, theoretical results of characterization and taking into account the temperature in which the catalysts were obtained (500°C), we suggested that the model MgO:AlZn(001)-T4-D is a reasonable proposal for the catalyst structure, taking into account the difficulty in the characterization. Thus, information extracted from this model can help the discussions of the experimental results.

3. Synthesis and characterization of azoxybenzenes

The followed mild conditions it were employed as the best reaction system for the synthesis of azoxybenzene compounds: 2 equivalents of oxidizing agent (H_2O_2), solvent ratio MeOH/H_2O_2 1:1 v/v, room temperature, violet LED light, **NbCat-02** catalyst, for 48 hours.

Table S2. Data of azoxybenzenes derived from anilines.

Compounds	δ H_{orto} / ppm	δ C-N+(O-)=N-Ar	υ-N+(O-)=N-	M.P. (°C)	Conversion*	Yield
1	8.38 (dd)	148.41	1474	35.0-36.0	95%	90%
2	8.35 (d)	144.3	1468	90.2-91.3	90%	85%
3	8.20 (dd)	147.09	1480	170.0-172.0	73%	60%
4	7.55 (ddd)	144.5	1444	99.0-100.0	97%	90%
5	8.27 (dd)	146.6	1473	152.5-154.3	98%	92%
6	8.60 (m)	134.2	1453	103.5-106.3	90%	80%
7	8.20 (dt)	146.3	1455	68.0-70.0	98%	89%
8	8.07 (d)	149.5	1449	58.0-59.0	98%	90%
9	8.12 (dd)	139.14	1435	81.0-82.0	91%	85%
10	8.47 (d)	150.2	1483	69.0-72.0	98%	89%
11	8.45 (dd)	150.9	1502	102.2-105.3	60%	55%
12	8.50 (dd)	149.96	1465	202.0-204.0	23%	15%
13	8.35 (d)	153.60	1460	>300.0	95%	85%
14	7.74 (m)	147.90	1480	247.0-249.0	90%	78%

* Based on ^{1}H NMR analysis of the crude reaction mixture.

- Characterization of azoxybenzene – **1**

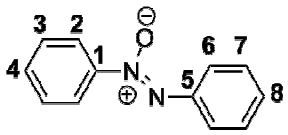

M.P.: 35-37°C

^{1}H NMR (500 MHz, $CDCl_3$), δ (ppm), *J* (Hz): 7.42 (t, 1H, H-4, $J_{p,m}$ = 7.0 Hz), 7.51-7.59 (m, 5H, H-3, H-7 and H-8), 8.27 (d, 2H, H-6, $J_{o',m'}$ = 8.0 Hz), 8.37 (d, 2H, H-2, $J_{o',m'}$ = 8.0 Hz).

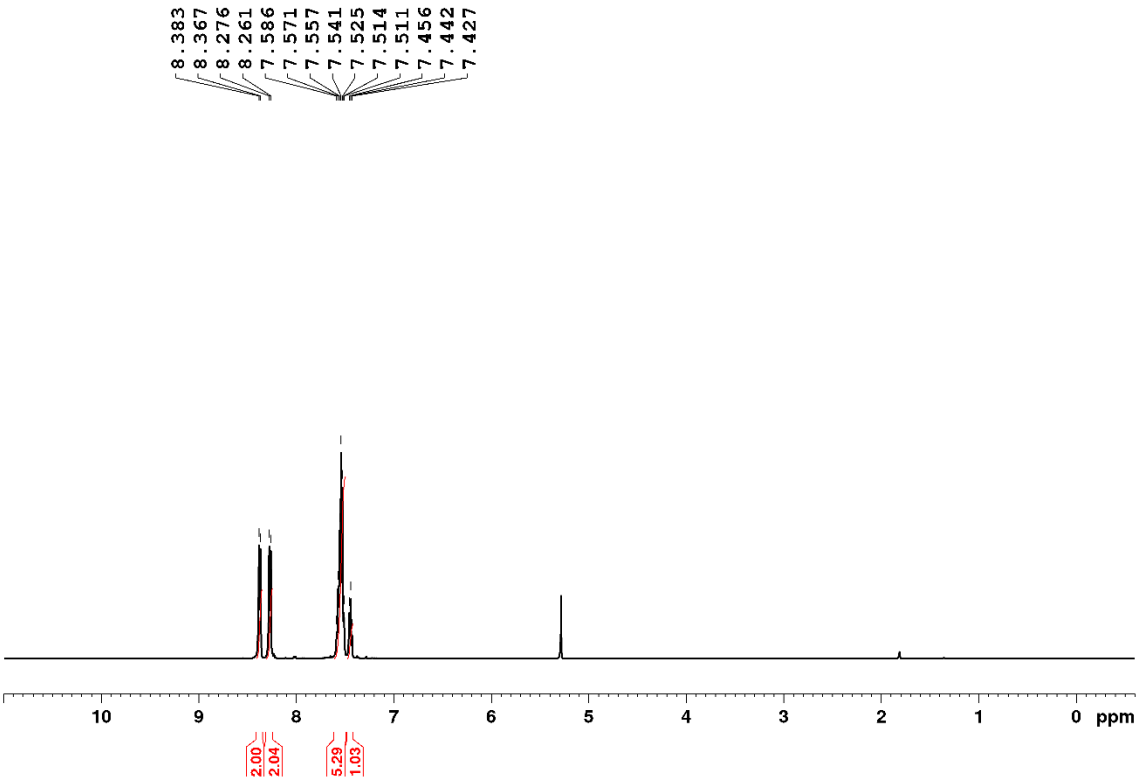

^{13}C NMR (125 MHz, $CDCl_3$), δ (ppm): 122.4 (C-6), 126.7 (C-2), 128.8, 128.9 (C-3 and C-7), 129.7 (C-4), 131.7 (C-8), 144.13 (C-1), 148.41 (C-5).

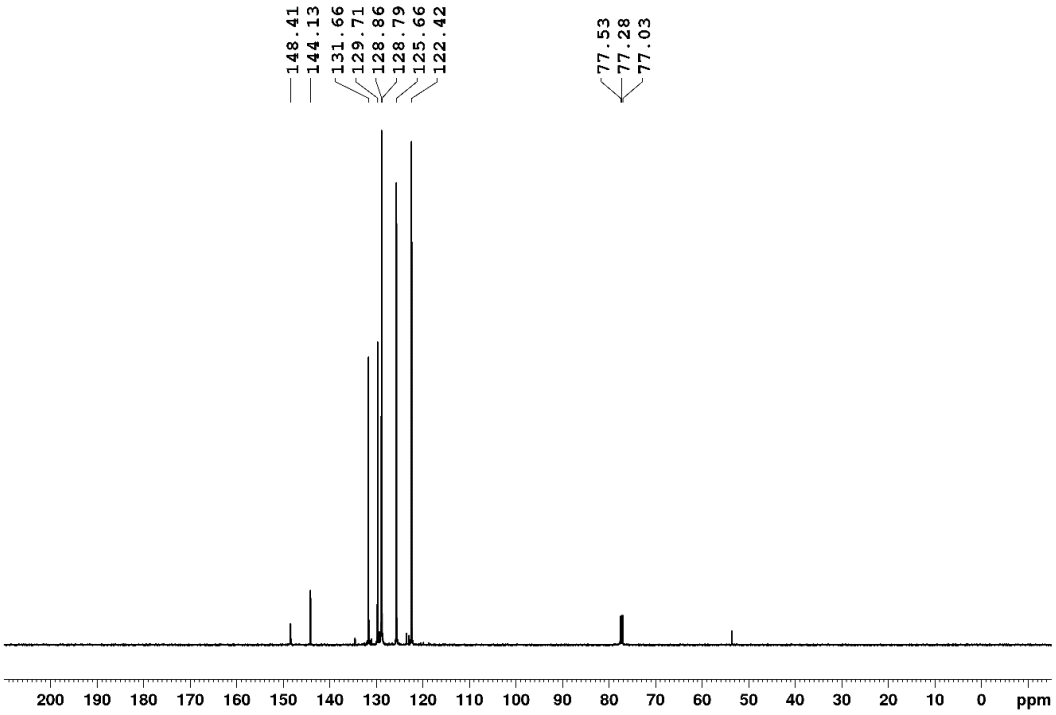

I.R. (KBr), (cm^{-1}): 3062 (CH aromatic stretching), 1472 ($N=N^{+}-O^{-}$ stretching), 757 (aromatic ring deformation).

- Characterization of 4,4'-di-fluoro-azoxybenzene – **2**

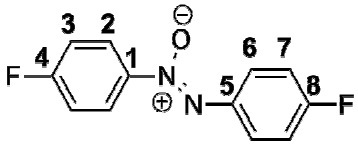

M.P.: 90.2-91.3 °C

^{1}H NMR (500 MHz, $CDCl_3$), δ (ppm), *J* (Hz): 7.17-7.22 (m, 4H, H-3 and H-7), 8.27 (dd, 2H, H-6, J_1 = 2.5 Hz, J_2 = 4.0 Hz), 8.2 (dd, 2H, H-2, J_1 = 4.5 Hz, J_2 = 7.0 Hz).

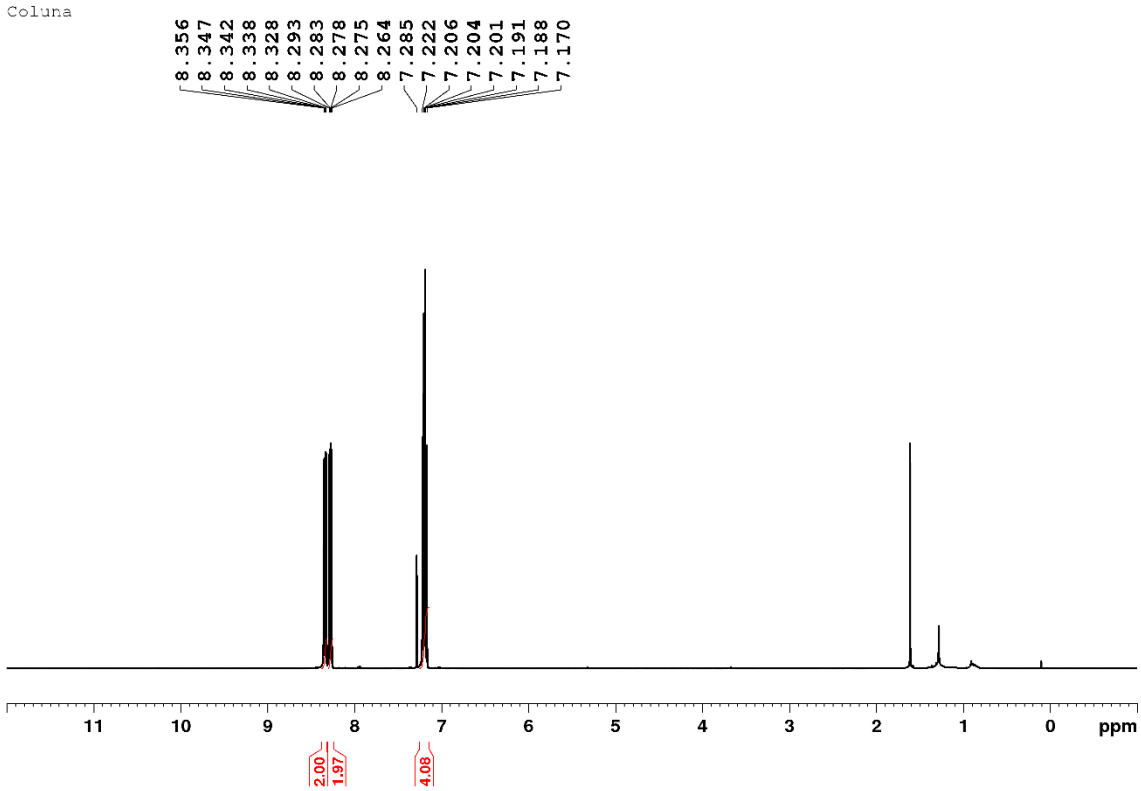

^{13}C NMR (125 MHz, $CDCl_3$), δ (ppm): 115.6, 115.8 (C-3 and C-7), 124.5 (C-2), 128.0 (C-6), 140.3 (C-5), 144.3 (C-1), 161.6, 163.5 (C-8, *J* = 98.5 Hz), 163.6, 165.5 (C-4, *J* = 98.0 Hz).

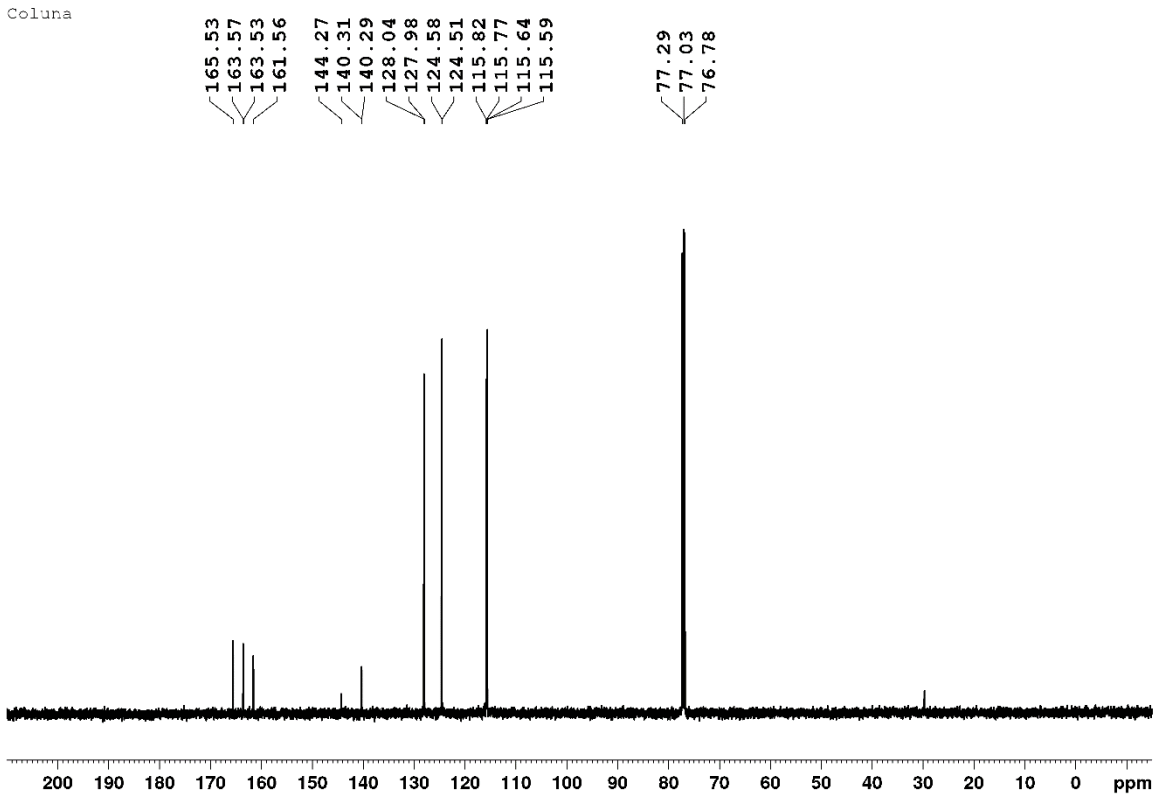

I.R. (KBr), (cm^{-1}): 3096 (aromatic CH stretching), 1468 ($N=N^{+}-O^{-}$ stretching), 841 (aromatic ring deformation).

- Characterization of 4,4'-di-bromo-azoxybenzene – **3**

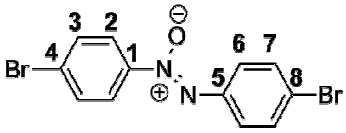

M.P.: 170.0-172.0°C °C

^{1}H NMR (500 MHz, $CDCl_3$), δ (ppm), *J* (Hz): 7.61-7.67 (dd, 2H, H-3 and H-7), 8.1 (dd, 2H, H-6, J_1 = 3.0 Hz, J_2 = 5.0 Hz), 8.2 (dd, 2H, H-2, J_1 = 3.0 Hz, J_2 = 5.0 Hz).

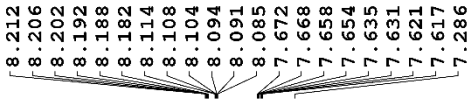

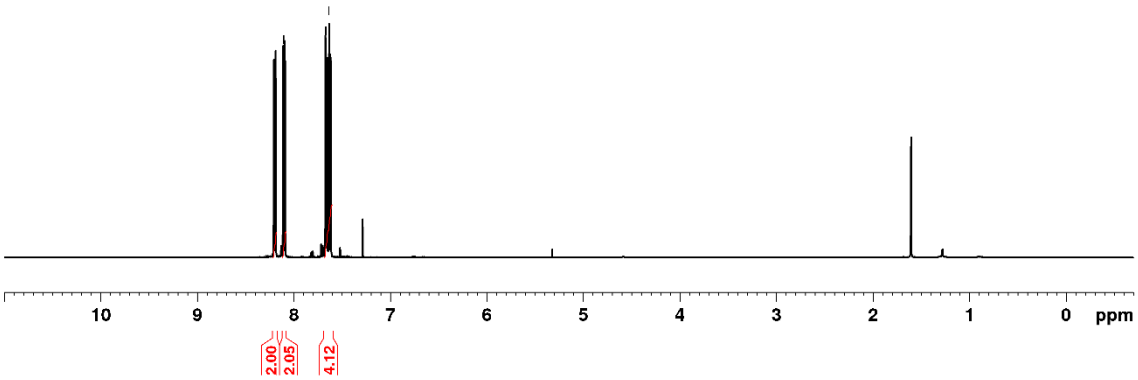

^{13}C NMR (125 MHz, $CDCl_3$), δ (ppm): 123.92 (C-2), 127.24 (C-6), 131.99 (C-3), 132.06 (C-7), 142.63 (C-5), 147.09 (C-1).

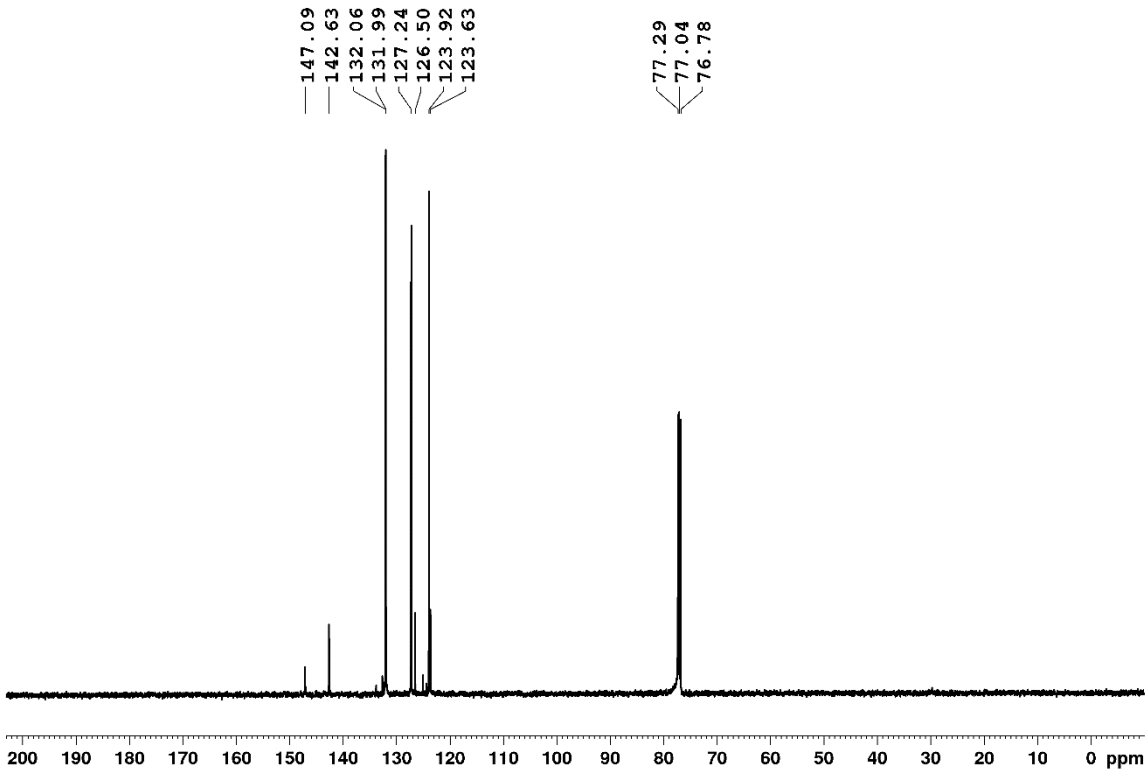

I.R. (KBr), (cm^{-1}): 3003 (aromatic CH stretching), 1458 ($N=N^{+}$-O^{-} stretching), 826 (aromatic ring deformation).

- Characterization of 3,3'-di-chloro-azoxybenzene – **4**

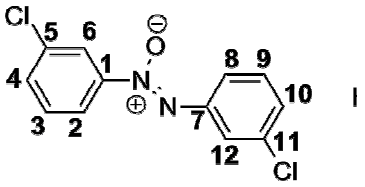

I

M.P.: 99,0-100,0 °C

^{1}H NMR (500 MHz, $CDCl_3$), δ (ppm), *J* (Hz): 7.29-7.47 (m, 5H, H-2, H-8, H-8, H-12), 7.54-7.56 (ddd, 1H, H-6, J_1 = 1.0 Hz, J_2 = 2.0 Hz, J_3 = 3.0 Hz), 7.99-8.02 (dt, 1H, H-10, J_1 = 1.5 Hz, J_2 = 3.5 Hz, J_3 = 7.5 Hz), 8.18-8.20 (ddd, 1H, H-4, J_1 = 1.0 Hz, J_2 = 2.0 Hz, J_3 = 3.0 Hz), 8.27 (dd, 1H, H-11, J_1 = 2.0 Hz e J_2 = 4.0 Hz), 8.30 (dd, 1H, H-5, J_1 = 2.0 Hz, J_2 = 4.5 Hz).

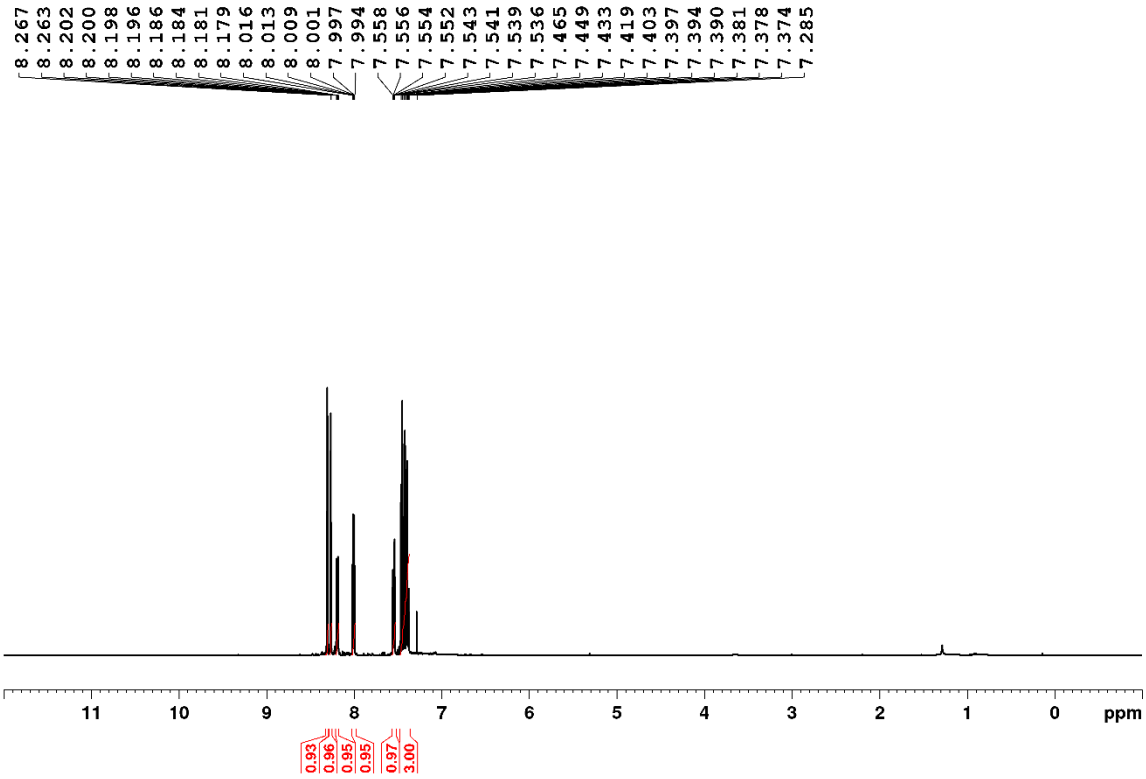

^{13}C NMR (125 MHz, $CDCl_3$), δ (ppm): 120.60 (C-4), 122.80 (C-5), 124.0 (C-10), 125.40 (C-11), 129.7, 129.9 (C-2, C-8, C-12), 132.01 (C-6), 134.40 (C-3), 134.82 (C-9), 144.5 (C-7), 148.80 (C-1).

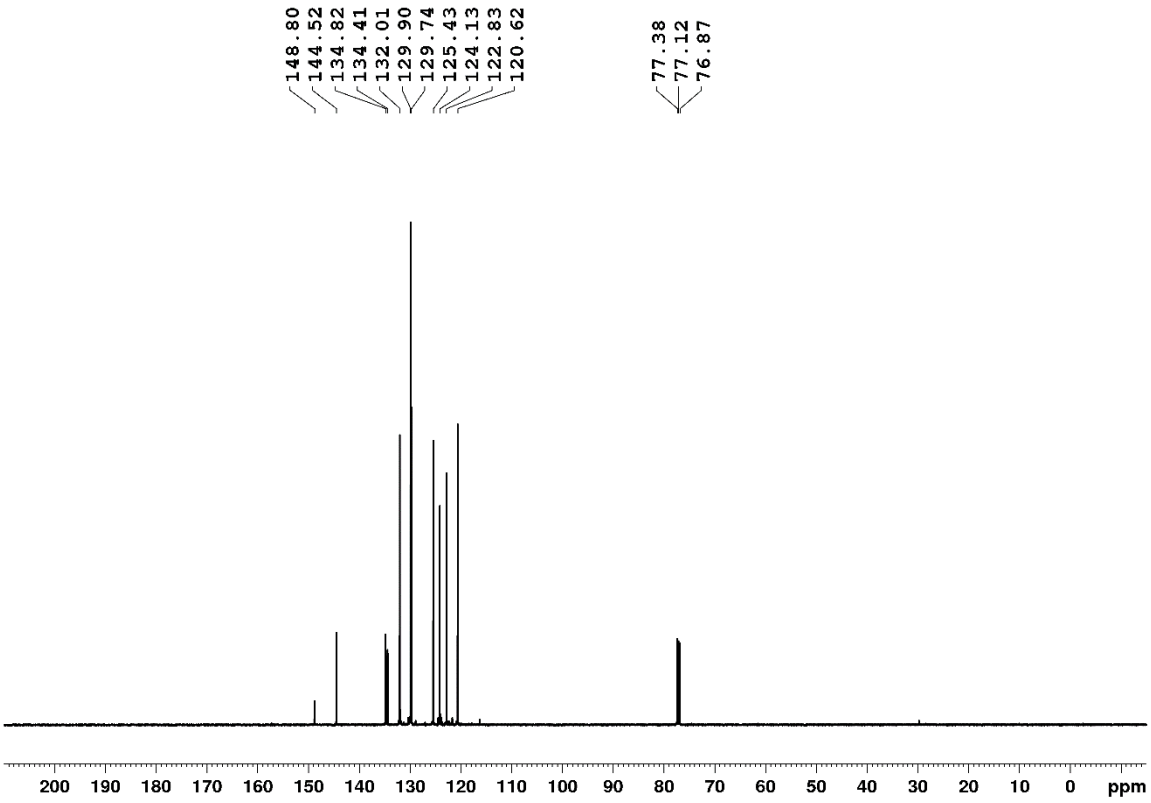

I.R. (KBr), (cm^{-1}): 3032 (aromatic C-H stretching), 1444 ($N=N^{+}-O^{-}$ stretching), 757 (aromatic ring deformation).

- Characterization of 4,4'-di-chloro-azoxybenzene – **5**

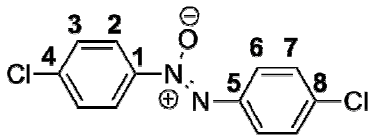

M.P.: 152.5-154.3 °C

^{1}H NMR (500 MHz, $CDCl_3$), δ (ppm), *J* (Hz): 7.45-7.52 (m, 4H, H-3, H-7), 8.18 (dd, 2H, H-6, J_1 = 3.0 Hz, J_2 = 5.0 Hz), 8.27 (dd, 2H, H-2, J_1 = 3.0 Hz, J_2 = 5.0 Hz).

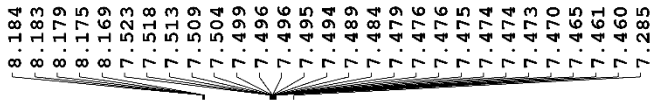

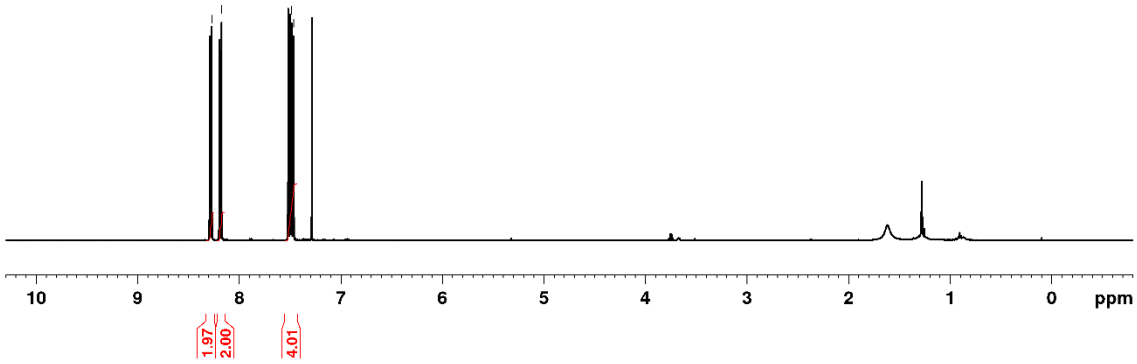

^{13}C NMR (125 MHz, $CDCl_3$), δ (ppm): 123.7 (C-2), 127.1 (C-6), 128.9, 129.1 (C-3, C-7), 135.3 (C-8), 138.1 (C-4), 142.2 (C-5), 146.6 (C-1).

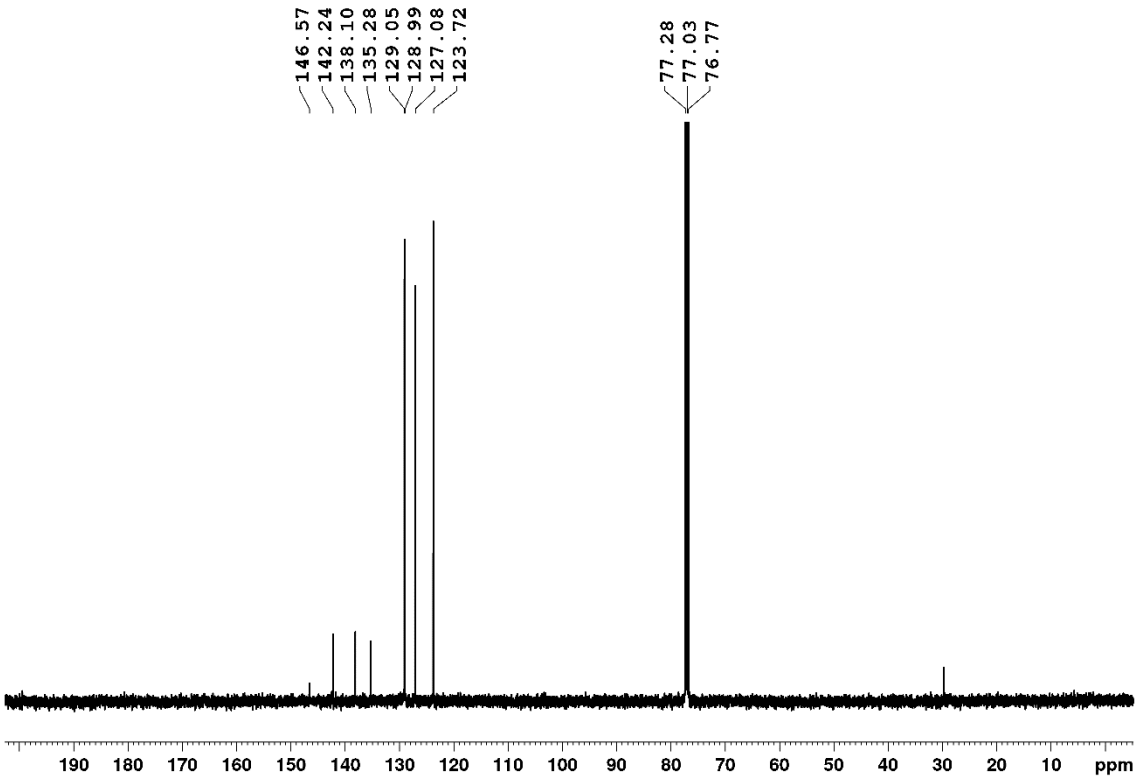

I.R. (KBr), (cm^{-1}): 3076 (aromatic CH stretching), 1473 ($N=N^{+}-O^{-}$ stretching), 752 (aromatic ring deformation).

- Characterization of 2,2'-4,4'-di-fluoro-azoxybenzene – **6**

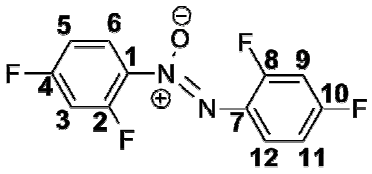

M.P.: 103.5-106.3 °C

^{1}H NMR (500 MHz, $CDCl_3$), δ (ppm), *J* (Hz): 6.98-7.28 (m, 4H, H-3, H-5, H-9, H-11), 7.98-8.03 (m, 1H, H-6), 8.56-8.61 (m, 1H, H-12).

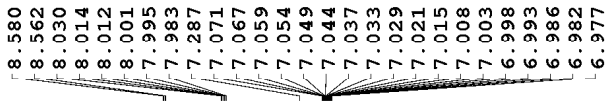

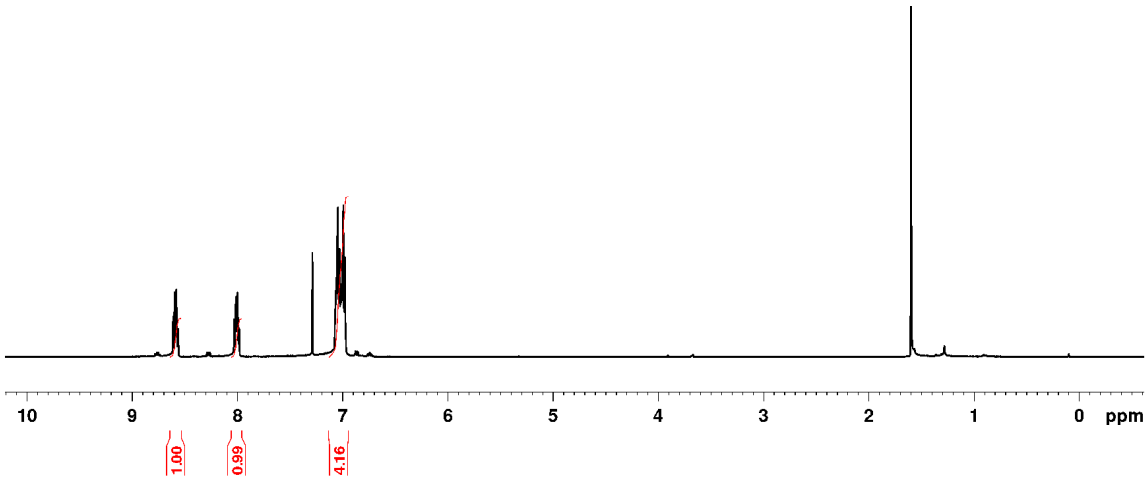

^{13}C NMR (125 MHz, $CDCl_3$), δ (ppm): 105.1, 111.8, 125.3, 127.1 (C-6, C-12, C-3, C-5, C-9, C-11), 129.1 (C-7), 134.2 (C-1), 154.4-164.8 (C-2, C-8, C-4, C-10).

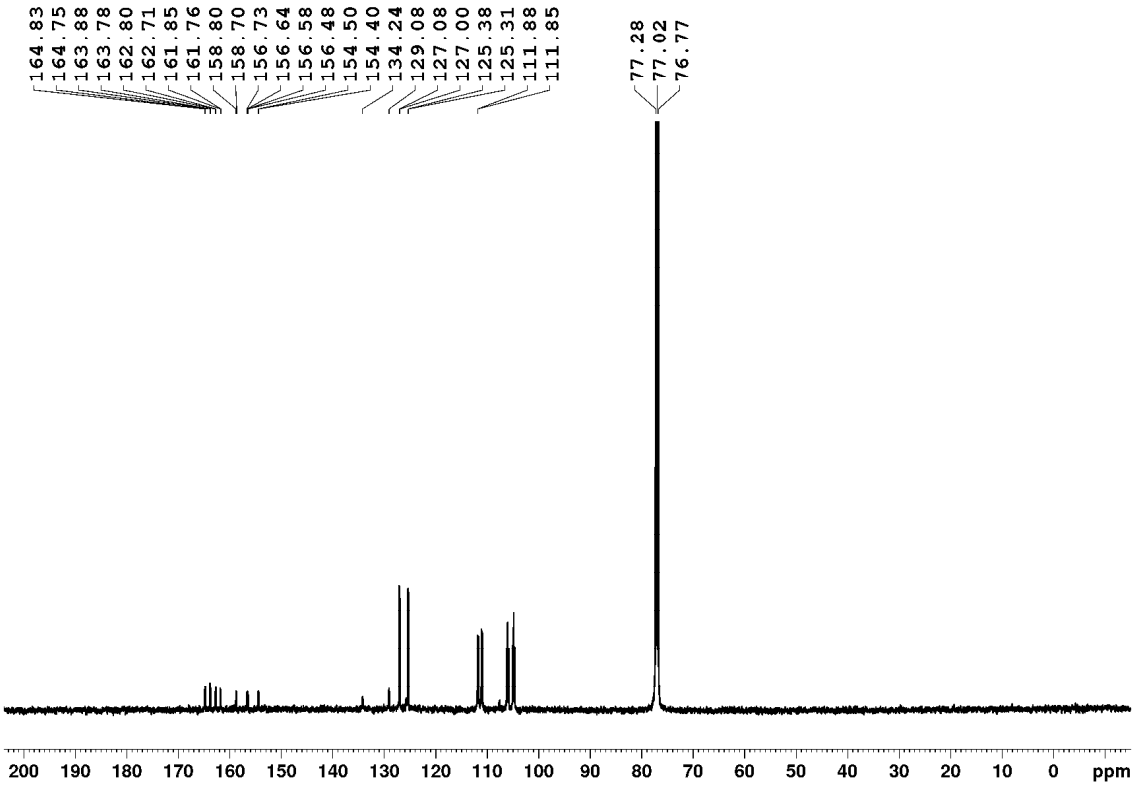

I.R. (KBr), (cm^{-1}): 3096 (aromatic CH stretching), 1453 ($N=N^{+}-O^{-}$ stretching), 826 (aromatic ring deformation).

- Characterization of 4,4'-di-methyl-azoxybenzene – **7**

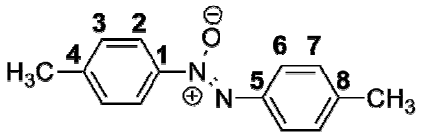

M.P.: 68.0-70.0 °C

^{1}H NMR (500 MHz, $CDCl_3$), δ (ppm), *J* (Hz): 2.44 (s, 3H, $C\underline{H}_3$), 2.47 (s, 3H, $C\underline{H}_3$), 7.28-7.32 (m, 4H, H-3, H-7), 8.15 (dt, 2H, J_1 = 2.5 Hz, J_2 = 4.5 Hz), 8.20 (dt, 2H, H-2, J_1 = 2.5 Hz, J_2 = 4.5 Hz).

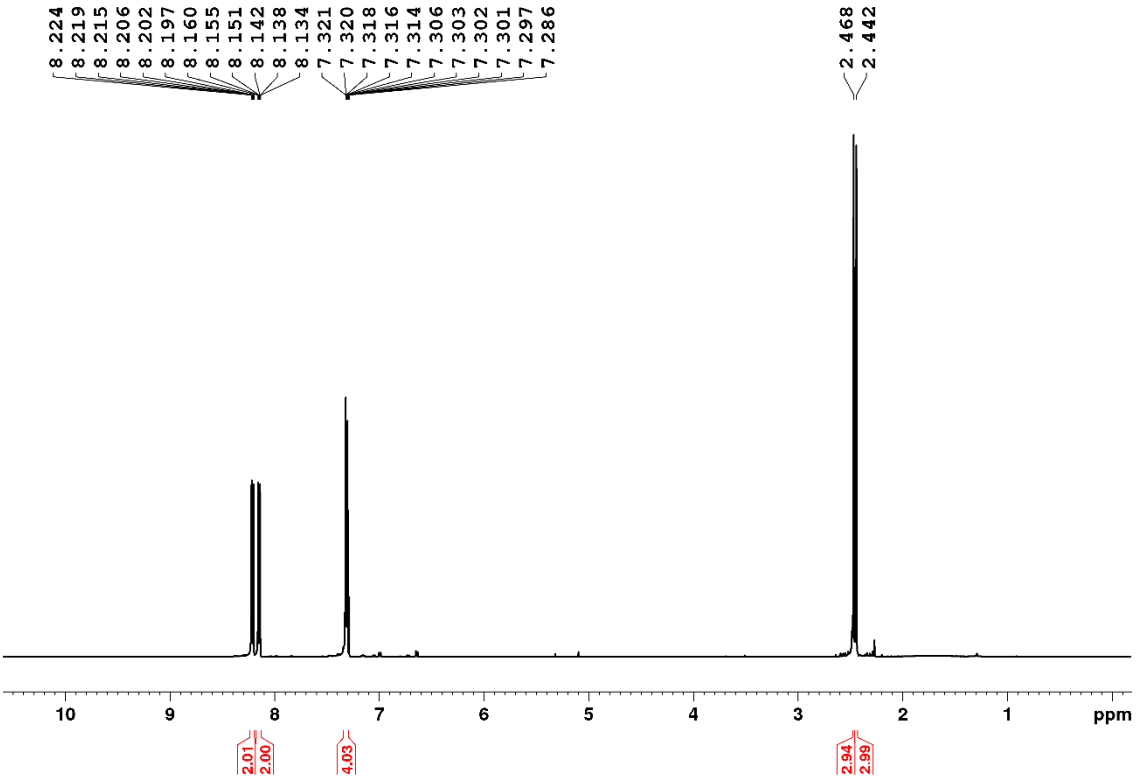

^{13}C NMR (125 MHz, $CDCl_3$), δ (ppm): 21.3 (CH_3), 21.6 (CH_3), 122.2 (C-2), 125.7 (C-6), 129.3 (C-3, C-7), 140.1 (C-8), 141.9 (C-4), 141.8 (C-5), 146.3 (C-1).

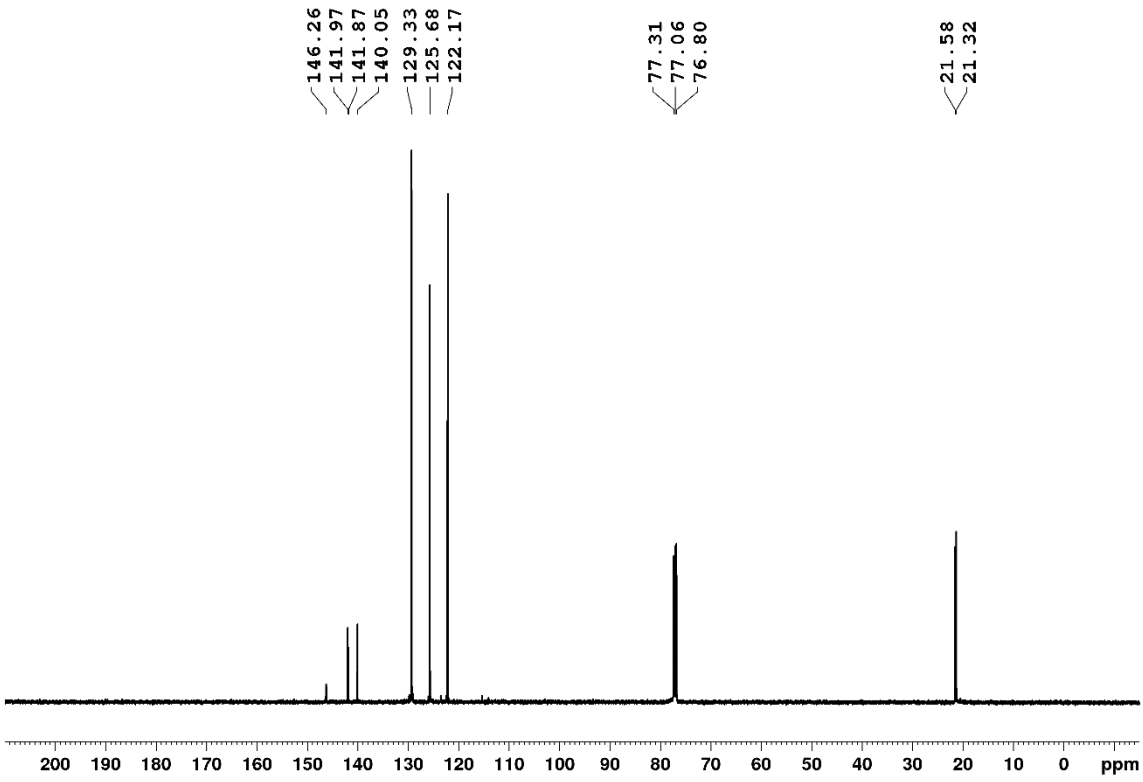

I.R. (KBr), (cm^{-1}): 3125 (aromatic CH stretching), 2995 (aliphatic CH stretching), 1463 ($N=N^{+}-O^{-}$ stretching), 811 (aromatic ring deformation).

- Characterization of 2,2'-di-methyl-azoxybenzene – **8**

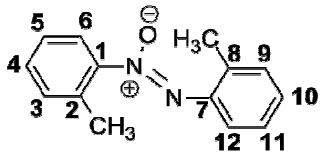

M.P.: 58.0-59.0 °C

^{1}H NMR (500 MHz, $CDCl_3$), δ (ppm), *J* (Hz): 2.41 (s, 3H, CH_3), 2.50 (s, 3H, CH_3), 7.28-7.37 (m, 5H, H-3, H-4, H-5, H-9 e H-11), 7.43 (t, 1H, H-10, J_1 = 6.5 Hz), 7.71 (d, 1H, H-12, J_1 = 8.5 Hz), 8.07 (d, 1H, H-6, J_1 = 8.0 Hz).

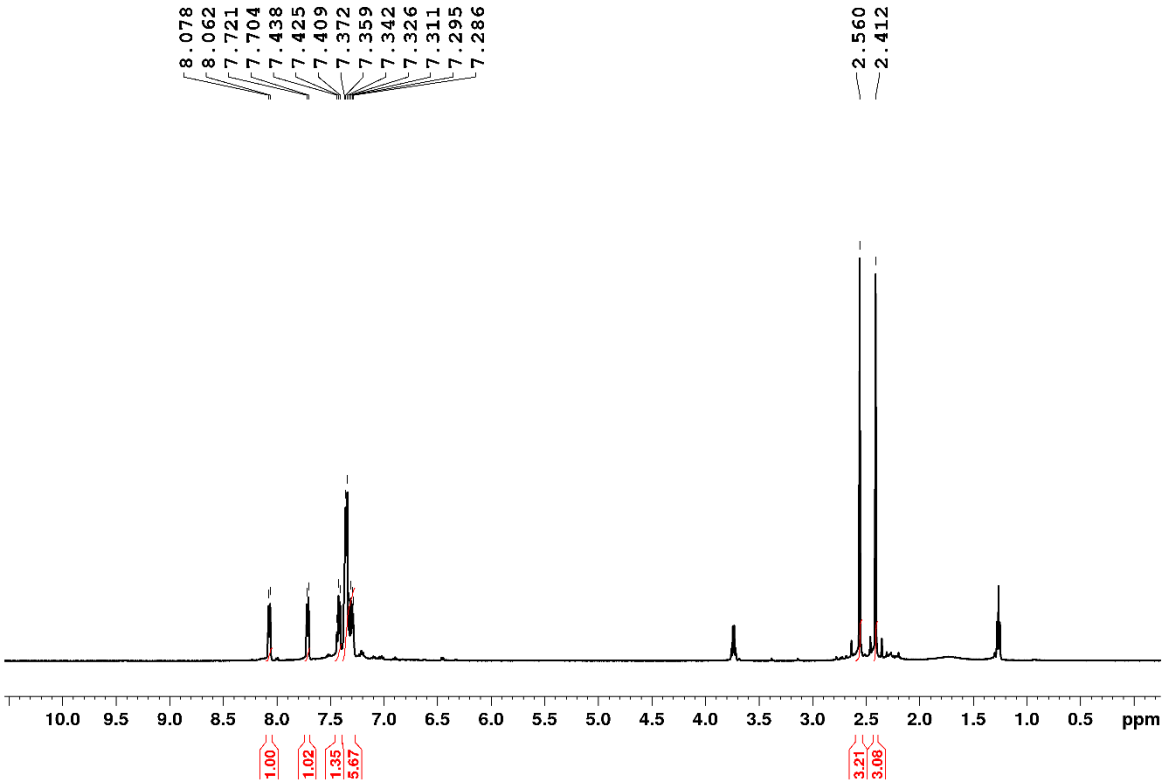

^{13}C NMR (125 MHz, $CDCl_3$), δ (ppm): 18.4 (CH_3), 18.5 (CH_3), 121.57 (C-6), 123.6 (C-12), 126.1 (C-3), 126.6 (C-4), 128.6 (C-5), 130.1 (C-11), 130.8 (C-10), 131.2 (C-8), 131.8 (C-9), 134.1 (C-2), 142.8 (C-5), 149.5 (C-1).

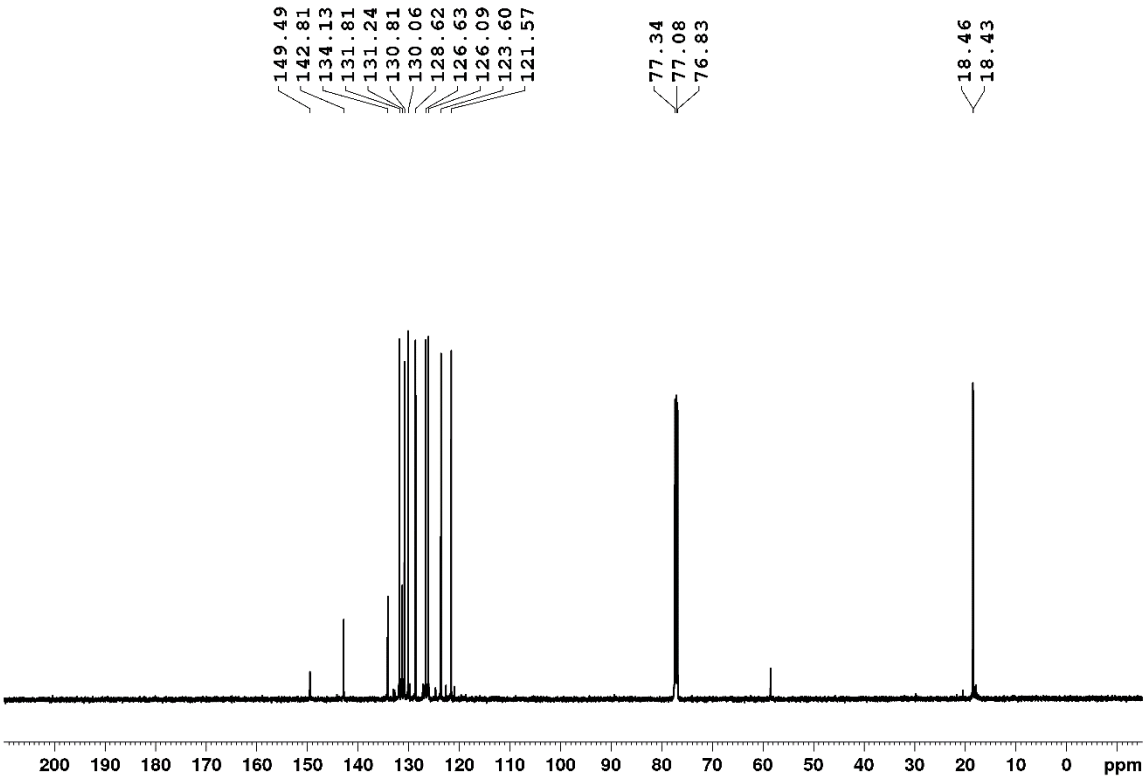

I.R. (KBr), (cm^{-1}): 2920 (aliphatic CH stretching), 1449 ($N=N^{+}-O^{-}$ stretching), 757 (aromatic ring deformation).

- Characterization of 2,2'-di-methoxy-azoxybenzene – **9**

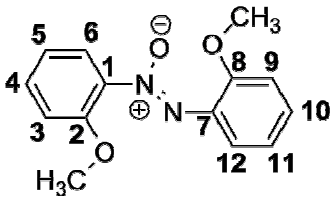

M.P.: 81.0-82.0°C

^{1}H NMR (500 MHz, $CDCl_3$), δ (ppm), *J* (Hz): 3.91 (s, 3H, CH_3), 3.93 (s, 3H, CH_3), 7.02-7.08 (m, 4H, H-3, H-5, H-9, H-11), 7.34 (ddd, 1H, H-10, J_1 = 1.5 Hz, J_2 = 8.5 Hz, J_3 = 7.5 Hz), 7.42 (ddd, 1H, H-4, J_1 = 2.0 Hz, J_2 = 8.5 Hz, J_3 = 7.5 Hz), 7.64 (dd, 2H, H-12, J_1 = 1.5 Hz, J_2 = 8.0 Hz), 8.12 (dd, 2H, H-6, J_1 = 1.5 Hz, J_2 = 7.5 Hz).

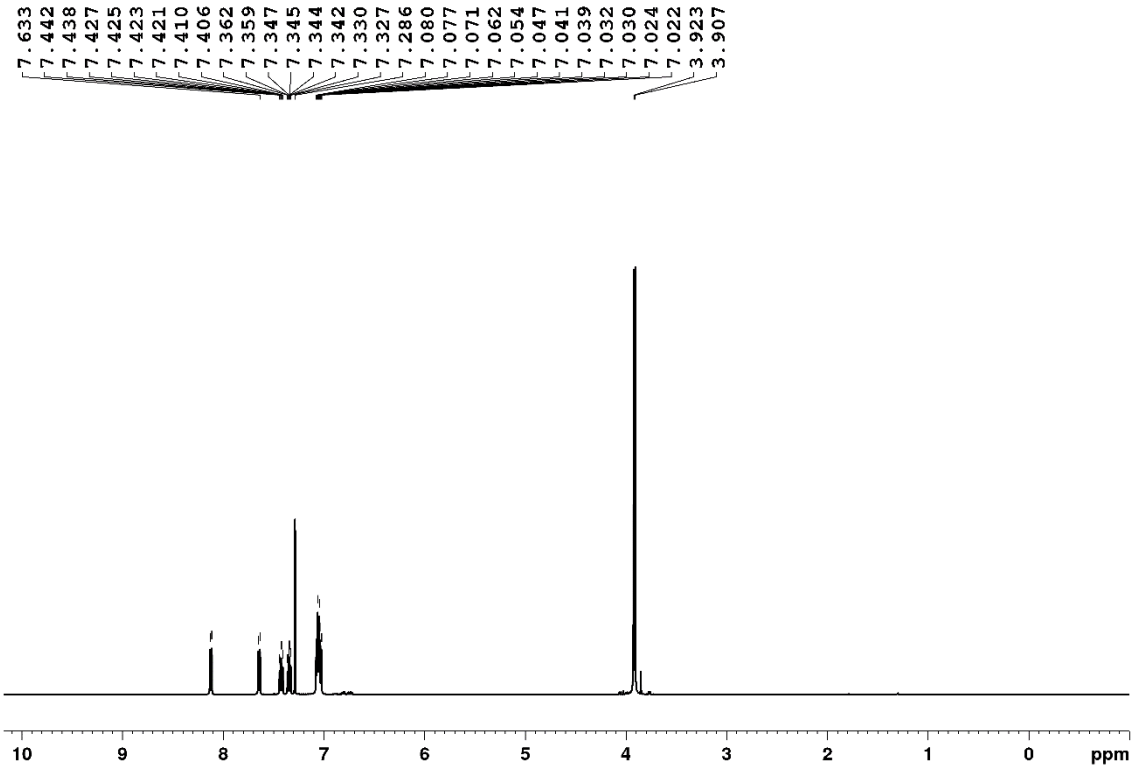

^{13}C NMR (125 MHz, $CDCl_3$), δ (ppm): 56.04 (CH_3), 56.38 (CH_3), 118.8 (C-9), 113.09 (C-3), 120.31 (C-5), 120.49 (C-11), 123.16 (C-6), 124.82 (C-12), 129.83 (C-10), 131.14 (C-4), 133.59 (C-7), 139.77 (C-1), 151.94 (C-8), 153.48 (C-2).

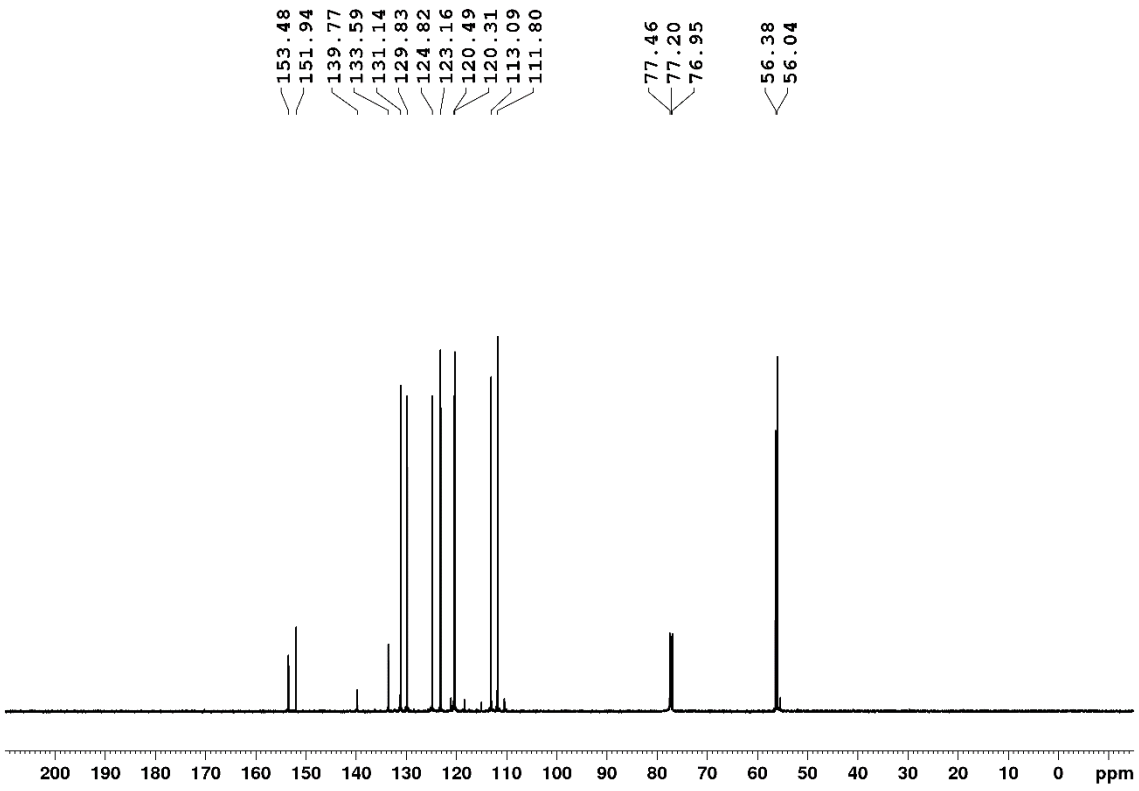

I.R. (KBr), (cm^{-1}): 3073 (aromatic CH stretching), 2944 (aliphatic C-H stretching), 1435 ($N=N^{+}-O^{-}$ stretching), 744 (aromatic ring deformation).

- Characterization of 4,4'-di-trifluoromethyl-azoxybenzene – **10**

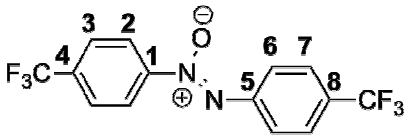

M.P.: 69.0-72.0 °C

^{1}H NMR (500 MHz, $CDCl_3$), δ (ppm), *J* (Hz): 7.78 (d, 2H, H-7, J_1 = 8.5 Hz), 7.83 (d, 2H, H-3, J_1 = 8.5 Hz), 8.25 (d, 2H, H-6, J_1 = 8.0 Hz), 8.47 (d, 2H, H-2, J_1 = 8.5 Hz).

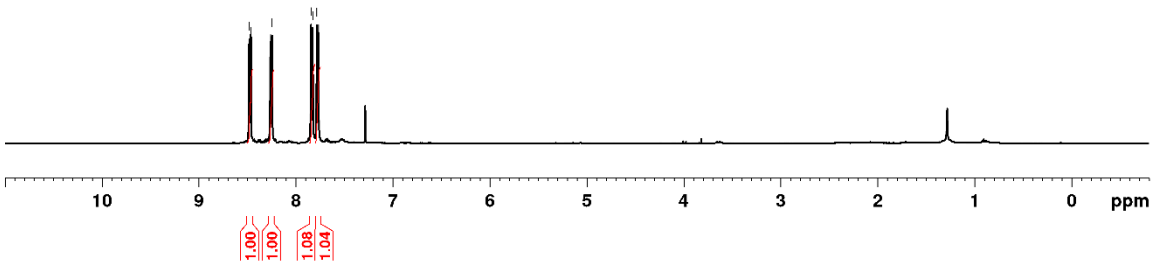

^{13}C NMR (125 MHz, $CDCl_3$), δ (ppm): 120.5 (C-8), 123.1 (C-2), 124.9 (C-4), 125.7 (C-6), 125.9 (C-7), 126.3 (C-3), 131.3 (CF_3), 134.1 (CF_3), 146.0 (C-5), 150.2 (C-1).

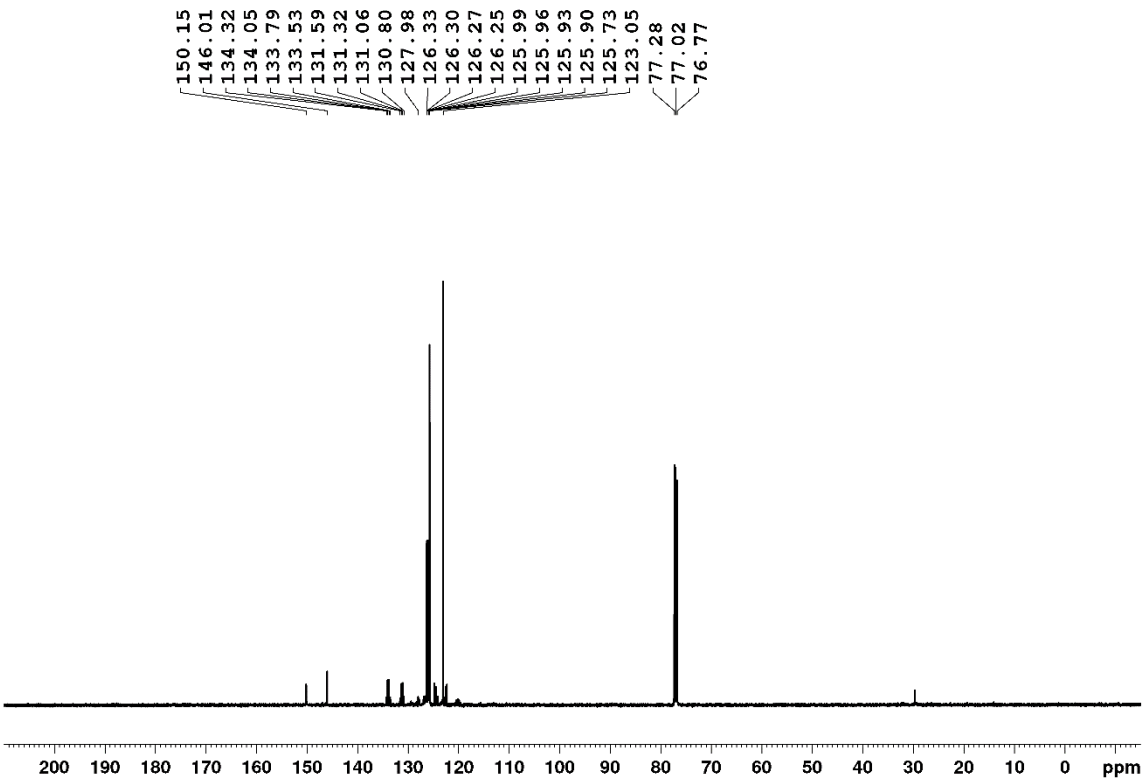

I.R. (KBr), (cm^{-1}): 3125 (aromatic CH stretching), 1463 ($N=N^{+}-O^{-}$ stretching), 846 (aromatic ring deformation).

- Characterization of 4,4'-di-sulphone-azoxybenzene – **11**

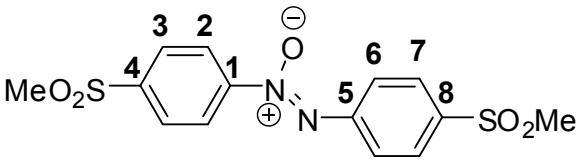

M.P.: 102.2-105.3°C

^{1}H NMR (500 MHz, $CDCl_3$), δ (ppm), *J* (Hz): 3.02 (s, 3H, CH_3), 3.14 (s, 3H, CH_3), 6.73 (dd, 2H, H-7, J_1 = 2.0 Hz, J_2 = 6.5 Hz), 7.72 (dd, 2H, H-6, J_1 = 2.0 Hz, J_2 = 7.0 Hz), 8.19 (dd, 2H, H-3, J_1 = 2.0 Hz, J_2 = 7.0 Hz), 8.45 (dd, 2H, H-2, J_1 = 2.0 Hz, J_2 = 6.5 Hz).

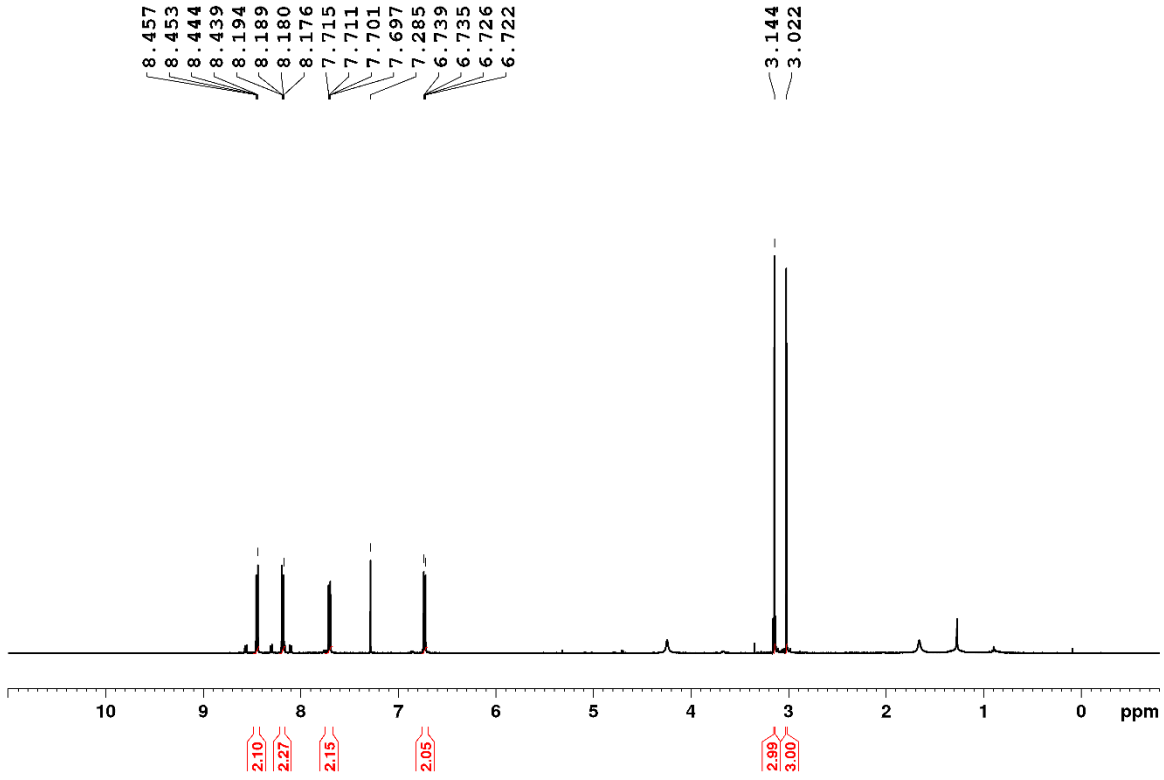

^{13}C NMR (125 MHz, $CDCl_3$), δ (ppm): 44.3 (CH_3), 44.9 (CH_3), 114.1 (C-7), 124.7 (C-6), 128.8 (C-5), 129.0 (C-2), 129.5 (C-3), 145.9 (C-4), 150.9 (C-1), 151.4 (C-8).

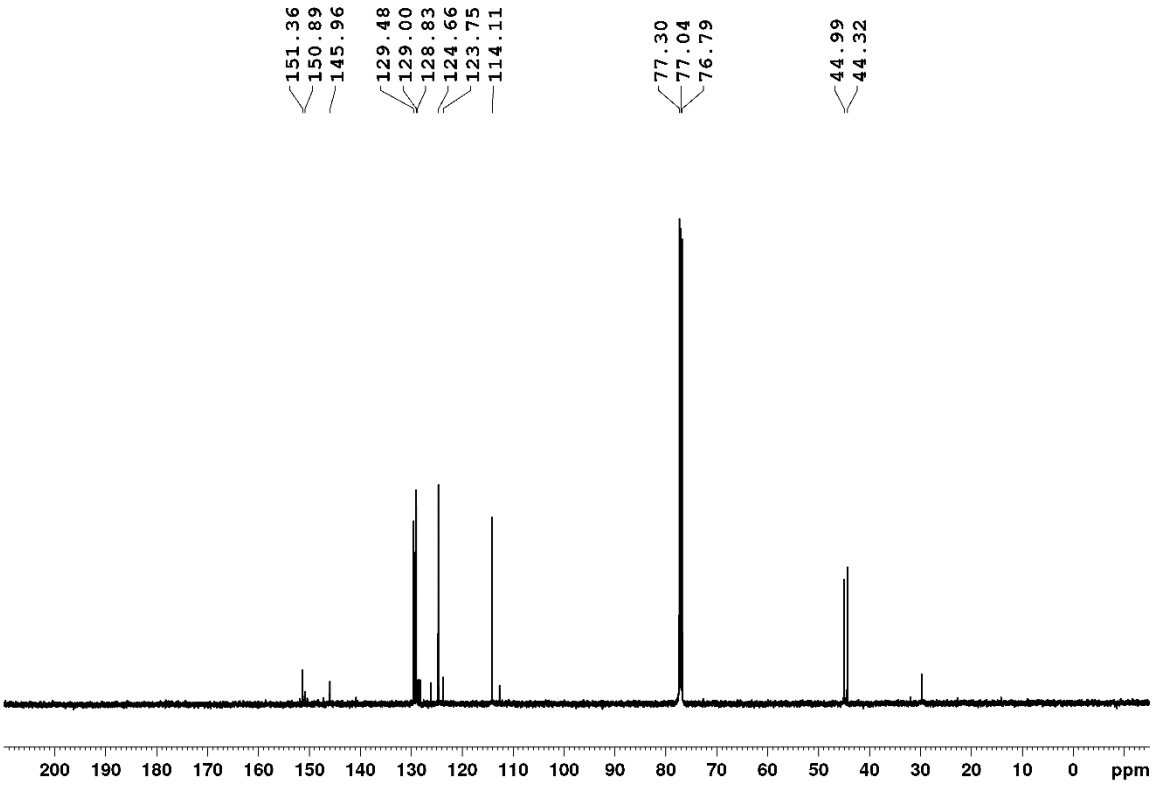

I.R. (KBr), (cm^{-1}): 2860 (aliphatic C-H stretching), 1502 ($N=N^{+}-O^{-}$ stretching), 1292 (asymmetric S=O stretching), 1135 (symmetric S=O stretching), 767 (aromatic ring deformation).

- Characterization of 4,4'-di-nitro-azoxybenzene – **12**

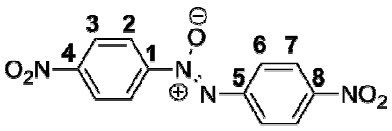

M.P.: 202.0-204.0°C

^{1}H NMR (500 MHz, $CDCl_3$), δ (ppm), *J* (Hz): 8.30 (m, 2H, H-6), 8.40 (m, 2H, H-7), 8.44-8.46 (m, 2H, H-3), 8.55 (m, 2H, H-2).

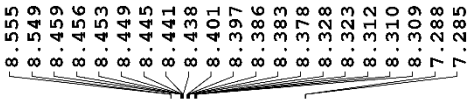

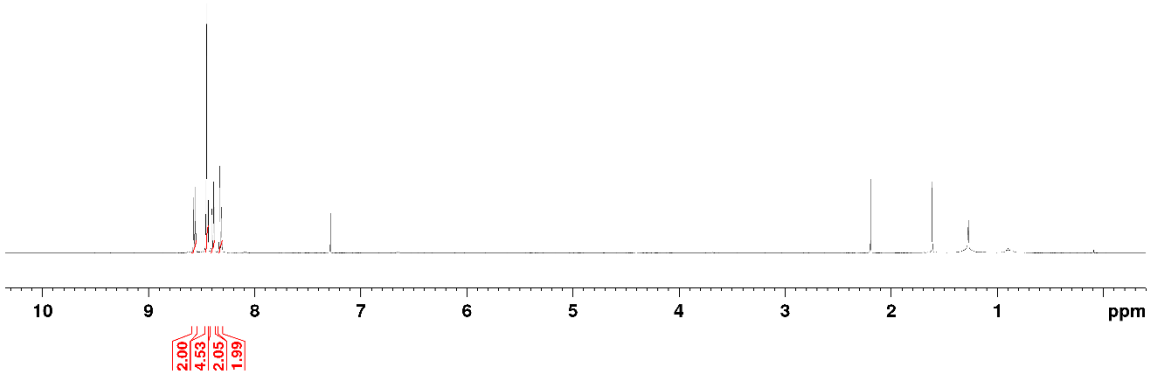

^{13}C NMR (125 MHz, $CDCl_3$), δ (ppm): 123.9 (C-2), 124.4 (C-7), 124.6 (C-3), 126.3 (C-6), 147.5 (C-4), 147.8 (C-5), 149.9 (C-8), 151.4 (C-1).

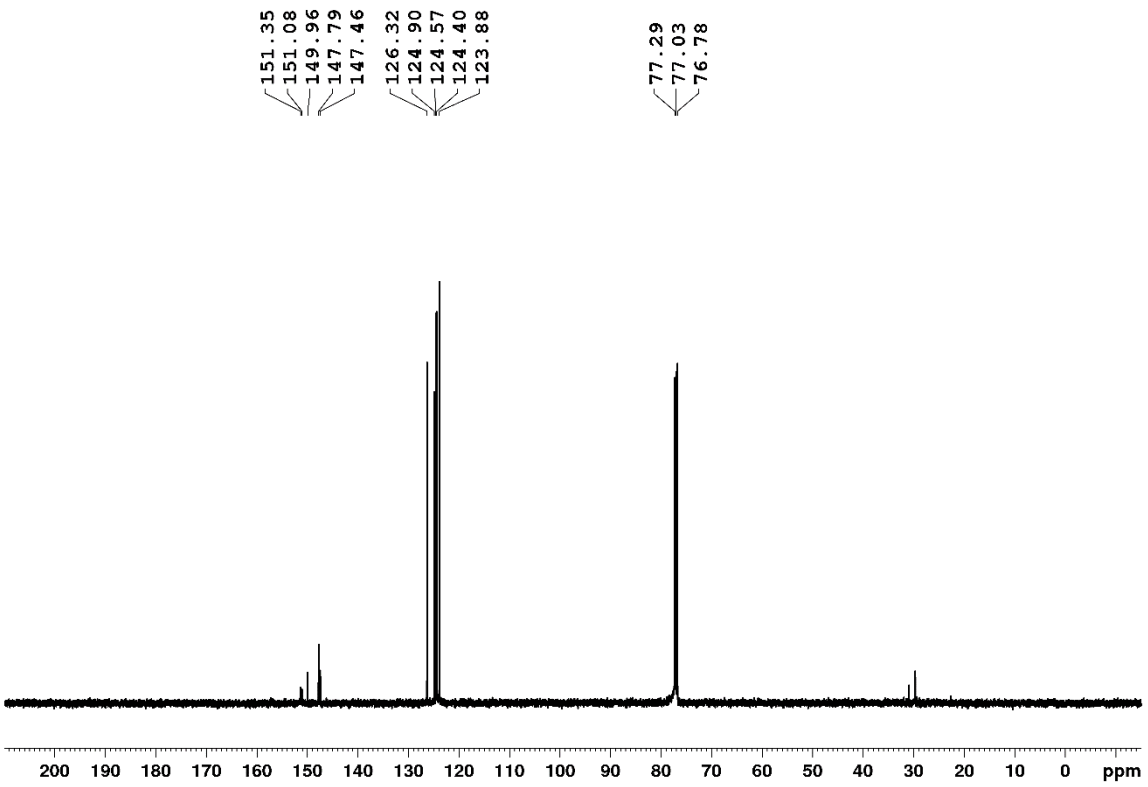

I.R. (KBr), (cm^{-1}): 3104 (aromatic CH stretching), 1465 ($N=N^{+}-O^{-}$ stretching), 1340 (N=O stretching), 747 (aromatic ring deformation).

- Characterization of 4,4'-di-carboxy-azoxybenzene – **13**

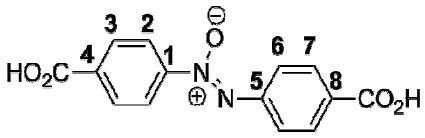

M.P.: > 300.0 °C

^{1}H NMR (500 MHz, $CDCl_3$), δ (ppm), *J* (Hz): 8.11-8.17 (m, 6H, H-6, H-3, H-7), 8.35 (d, 2H, H-2, J_1 = 8.5 Hz), 13.38 (br, 2H, CO_2H).

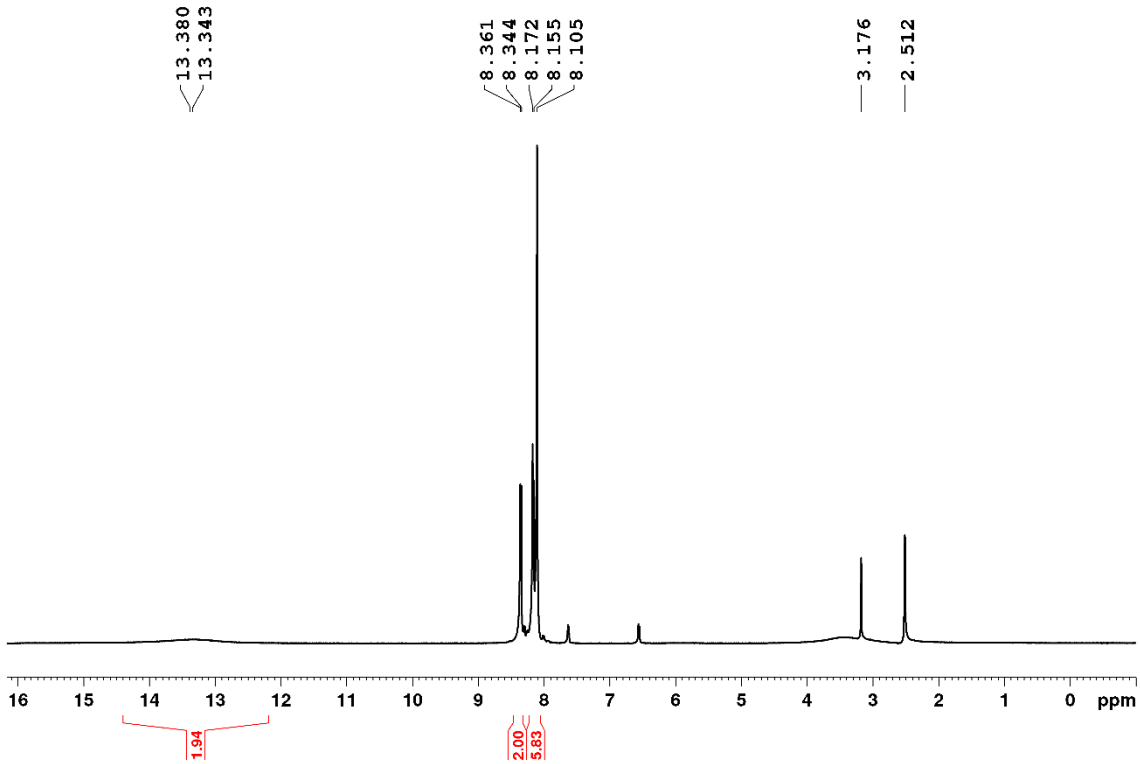

^{13}C NMR (125 MHz, $CDCl_3$), δ (ppm): 122.9 (C-2), 125.4 (C-7), 130.5 (C-3), 130.9 (C-6), 131.9 (C-5), 134.9 (C-1), 146.9 (C-8), 150.5 (C-4), 166.9 (CO_2H), 167.1 (CO_2H).

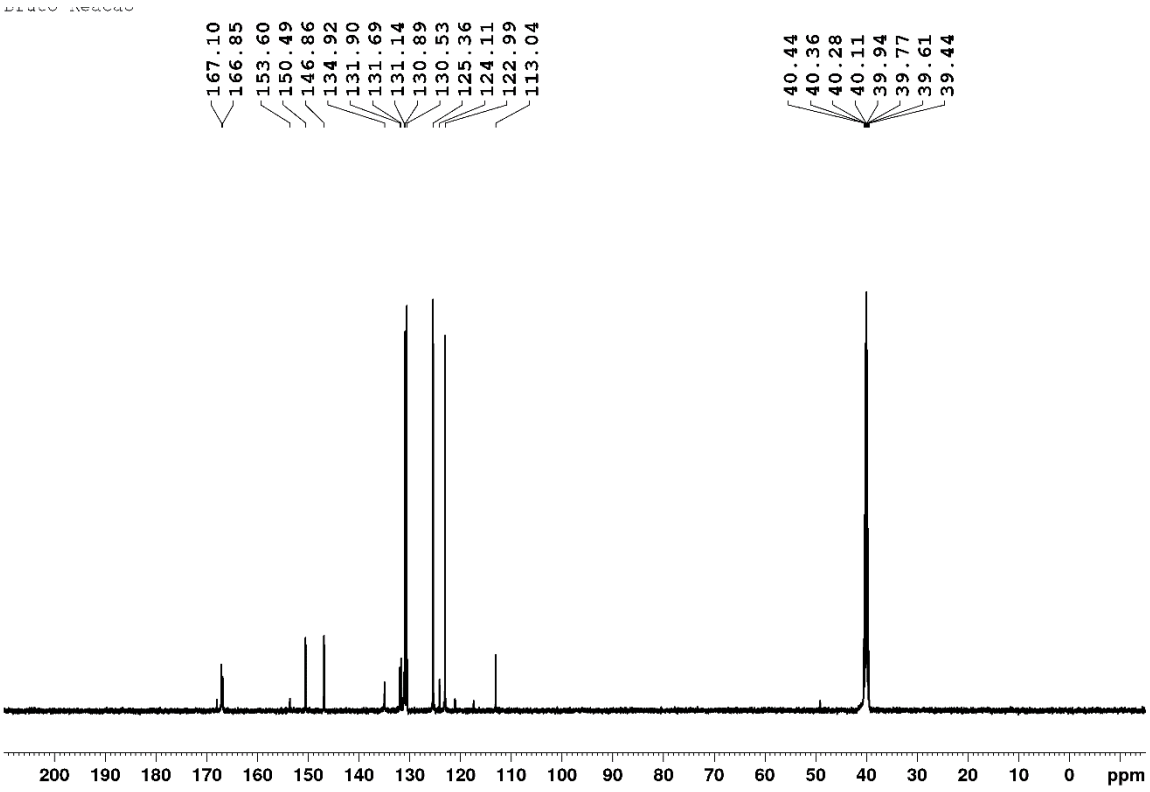

I.R. (KBr), (cm^{-1}): 1691 (C=O stretching), 1460 ($N=N^{+}-O^{-}$ stretching), 770 (aromatic ring deformation).

- Characterization of 2,2'-di-carboxy-azoxybenzene – **14**

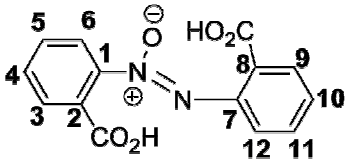

M.P.: 247.0-249.0 °C

^{1}H NMR (500 MHz, $CDCl_3$), δ (ppm), *J* (Hz): 7.26 (d, 1H, H-12, J_1 = 8.0 Hz), 7.48-7.45 (m, 1H, H-4), 7.74-7.69 (m, 2H, H-6, H-10), 7.78-7.86 (m, 2H, H-5, H-11), 7.90 (dd, 1H, H-9, J_1 = 8.0 Hz, J_2 = 8.5 Hz), 7.97 (dd, 1H, H-3, J_1 = 8.0 Hz, J_2 = 8.5 Hz).

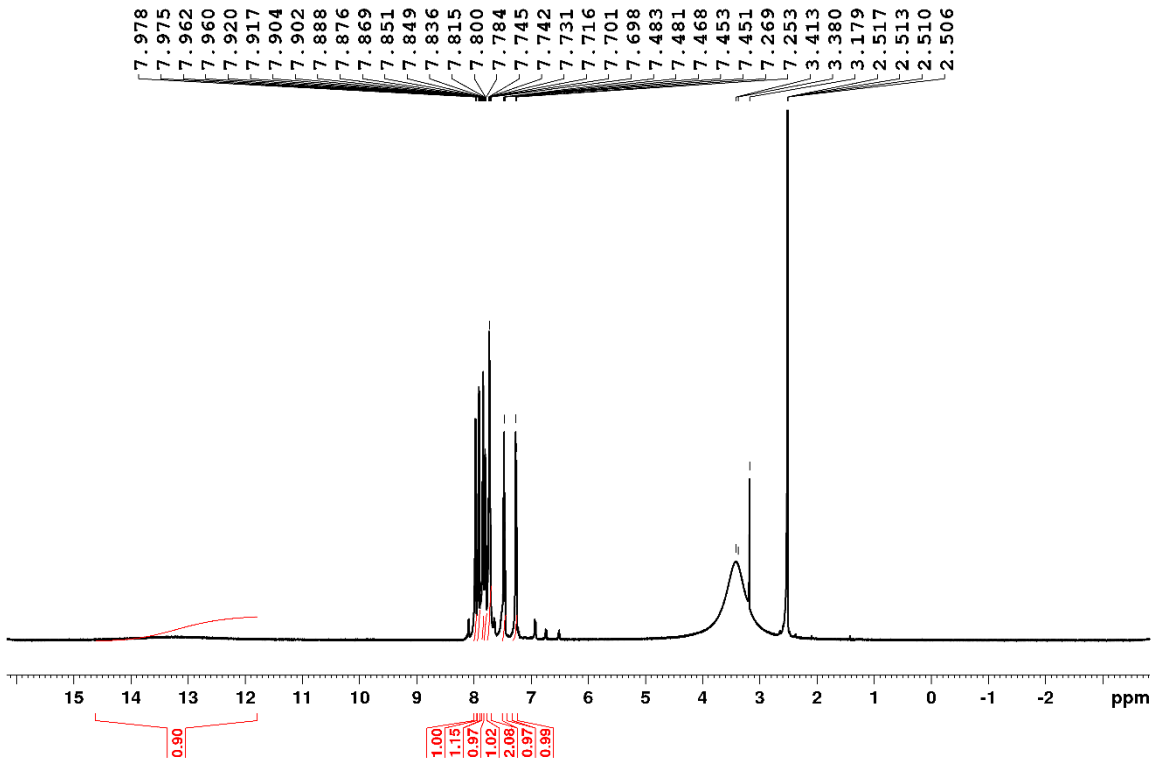

^{13}C NMR (125 MHz, $CDCl_3$), δ (ppm): 122.5 (C-12), 123.9 (C-5), 125.2 (C-8), 127.3 (C-2), 127.8 (C-4), 130.6 (C-9), 130.8 (C-3), 131.3 (C-6), 132.8 (C-11), 133.3 (C-10), 144.7 (C-7), 147.9 (C-1), 166.7 (CO_2H), 167.0 (CO_2H).

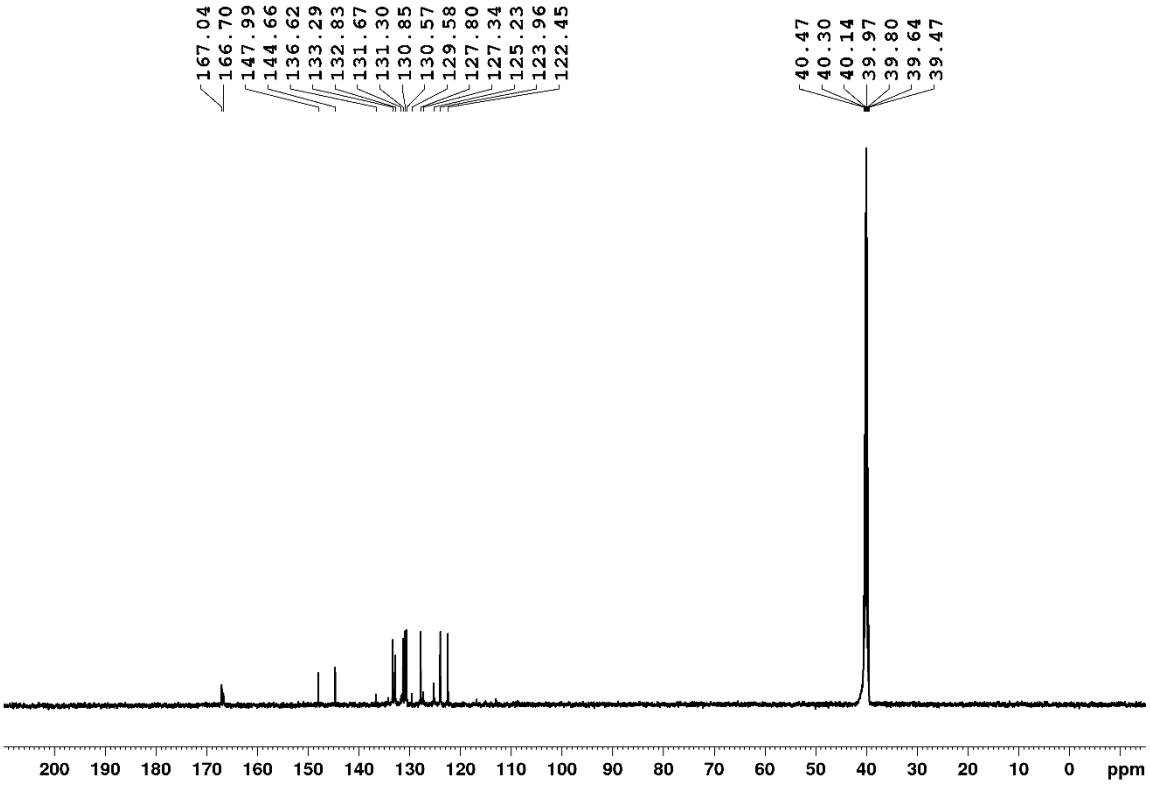

I.R. (KBr), (cm^{-1}): 1684 (C=O stretching), 1488 ($N=N^{+}-O^{-}$ stretching), 757 (aromatic ring deformation).

References

[1] R. M. Hazen, *Am. Mineral.* **1976**, *61*, 266–271.

[2] A.V. Chichagov Kristallographiya, v.35, n.3 (1990) p.610-616 (in Russian)

[3] R. S. Alvim, V. S. Vaiss, A. A. Leitão, I. Borges, Jr., *J. Phys. Chem.* **2013**, *117*, 20791−20801.

[4] S. Baroni, S. de Gironcoli, A. Dal Corso, P. Giannozzi, *Rev. Mod. Phys.* **2001**, *73*, 515.

[5] J-.M. Jheng, I. E. Wachs, *J . Phys. Chem.* **1991**, *95*, 7373-7379.

[6] H. Guesmi, R. Grybos, J. Handzlik, F. Tielens, *RSC Adv.* **2016**, *6*, 39424–39432.

[7] D.C. Tranca, A. Wojtaszek-Gurdak, M. Ziolekb, F. Tielens, *Phys. Chem. Chem. Phys.* **2015**, *17*, 22402-22411.

[8] J. Z. Hu, J. H. Kwak, Y. W., M. Y. Hu, R. V. Turcu, C. H. F. Peden, *J. Phys. Chem. C* **2011**, *115*, 23354–23362.

[9] M. M. Islam, D. Costa, M. Calatayud, F. Tielens, *J. Phys. Chem. C* **2009**, *113*, 10740–10746.

[10] L. J. Burcham, J. Datka, I. E. Wachs, *J. Phys. Chem. B* **1999**, *103*, 6015-6024.